Glauber Theory of Atomic Hydrogen Excitation by Electron Impact*

H. Tai, R. H. Bassel† and E. Gerjuoy

Department of Physics, University of Pittsburgh, Pittsburgh, Pennsylvania 15213

and

V. Franco††

Physics Department, Brooklyn College of the City University of New York, Brooklyn, New York 11210 and University of California, Los Alamos Scientific Laboratory, Los Alamos, New Mexico 87544.

Abstract

The Glauber approximation has been applied to excitation of the 2s, 2p, 3s and 3p levels of the hydrogen atom by electron impact. The differential and integrated excitation cross sections predicted by Glauber theory have been compared with experiment and with other calculations. The Glauber approximation is a considerable improvement over the Born approximation at energies $< \sim 100$ eV. At energies $> \sim 100$ eV the Glauber total excitation cross sections approach the Born, even though at large scattering angles ($> 40^{\circ}$) the Glauber differential cross sections may be very different from the Born. At intermediate energies (~ 30 eV - 100 eV) the Glauber predictions are surprisingly good; at energies $< \sim 20$ eV the Glauber integrated cross sections are rather smaller than observed experimentally.

† Present address, Naval Research Laboratory, Washington, D. C. 20390.

†† Present address, Brooklyn College, Brooklyn, New York 11210.

* Work supported in part by the Advanced Research Projects Agency under Contract No. DA-31-124-ARO-D-440, by the National Aeronautics and Space Administration under Contract No. NGR-30-011-035, and by the U. S. Atomic Energy Commission. The calculations for the 1s-2s transitions were performed independently by one of us (VF), who is not responsible for the numerical results on the 2p, 3s and 3p transitions. To avoid unnecessary proliferation of publication, we have decided to publish jointly.

1. Introduction

In the past, the Glauber[1] approximation for scattering amplitudes has been applied to many problems in particle physics and in nuclear physics[2]. More recently, the Glauber approximation has been employed in the elastic scattering of electrons by hydrogen atoms[3,4]. In these latter calculations--for angular distributions as well as for total elastic cross sections--the Glauber theory agrees surprisingly well with experiment, even at comparatively low electron energies ($< \sim 100$ eV) where Glauber's formulation might be expected to break down. As a matter of fact, Glauber's theory is essentially a diffraction approximation[5], wherein it is assumed that the incident plane wave sweeps virtually undeviated through the region of interaction and emerges suffering only a position-dependent change of phase and amplitude; obviously this assumption is likely to be invalid at low energies. On the other hand, the Glauber theory has the virtue--to which its aforementioned success in e-H elastic scattering perhaps can be ascribed--that it takes account of the interactions of the incident electron with both the target electron and the target proton; for excitation processes, in most other easily computed approximations, the interaction between the incident electron and the proton either produces identically zero scattering (first Born approximation, hereafter denoted by FBA), or else is assumed to produce negligible scattering (impulse approximation[6], Vainshtein approximation[7]).

In view of the preceding paragraph, it seems reasonable to examine the utility of Glauber theory in the inelastic scattering of atomic hydrogen by electrons, especially at energies < 100 eV, where FBA is known to be very poor (see section 4). The specific reactions examined by us include excitation of H(1s) to the 2s, 2p, 3s and 3p levels. The derivations of the

theoretical formulas employed are given in the two following sections. A fourth and final section discusses the results obtained, including their comparison with experiment.

2. Basic Formulas

In what follows, we suppose the target proton to be infinitely heavy. Also, we neglect exchange scattering, which is not readily estimated in a diffraction theory like Glauber's; the possible significance of this neglect will be discussed in the final section. Let $\hbar\vec{K}_i, \hbar\vec{K}_f \equiv m\vec{v}_i, m\vec{v}_f$ be respectively the momentum vectors of the incident electron before and after the collision, and define

$$\vec{q} = \vec{K}_i - \vec{K}_f$$

Place the origin of coordinates at the proton, with the z-axis (also the polar axis) along $\vec{K}_i$. Let $\vec{r}, \vec{r}'$ denote respectively the position vectors of the target and incident electrons, and write

$$\vec{r} = \vec{s} + \vec{z}$$

$$\vec{r}' = \vec{b} + \vec{\zeta}$$

where (see Fig. 1) $\vec{s}$ is the projection of $\vec{r}$ onto the x,y plane; correspondingly, the impact parameter vector $\vec{b}$ lies in the x,y plane, and is the perpendicular from the origin to the incident particle's initial trajectory.

With these definitions the amplitude $F_{fi}(\vec{q})$ for collisions in which

the atom undergoes a transition from an initial state i with wave function u_i to a final state f with wave function u_f, and in which the incident particle imparts a momentum $\hbar\vec{q}$ to the target is given by[1]

$$F_{fi}(\vec{q}) = \frac{iK_i}{2\pi}\int u_f^*(\vec{r})\ \Gamma(\vec{b},\vec{r})\ u_i(\vec{r})\ \exp(i\vec{q}\cdot\vec{b})\ d^2b\ d\vec{r} \qquad (1)$$

Moreover, in Eq. (1)

$$\Gamma(\vec{b},\vec{r}) = 1 - e^{i\chi(\vec{b},\vec{s})} \qquad (2)$$

with the phase shift function

$$\chi(\vec{b},\vec{s}) = -\frac{1}{\hbar v_i}\int_{-\infty}^{\infty} V(\vec{b},\vec{r},\zeta)\ d\zeta$$

the integral—along the trajectory of the incident electron—of the instantaneous potential between the incident particle and the target. For electrons incident on atomic hydrogen, one finds readily[3]

$$\chi(\vec{b},\vec{s}) = 2n \log\left(\frac{|\vec{b}-\vec{s}|}{b}\right) \qquad (3)$$

where $n = e^2/\hbar v_i$.

When the exponential in (2) is expanded in powers of χ, the first non-vanishing term in (1) is linear in χ, and can be seen to be identical with FBA. Retention of only the linear terms in χ should be valid at large v_i. Thus one might infer that the Glauber predictions for $F_{fi}(\vec{q})$

should merge with the FBA at sufficiently high incident energies. This inference is not really justified, however, for reasons which will be discussed in section 4 below. In particular, for the inelastic cross sections examined in this paper, the Glauber and FBA predictions at large scattering angles ($\sim 60^{\circ}$, for instance) apparently do not approach each other as the incident energy is increased. However, at high energies large angle scattering generally makes a relatively inconsequential contribution to integrated cross sections, whether elastic or inelastic. Therefore we do expect that the Glauber total (i.e., integrated over angle) inelastic cross sections will approach the FBA at sufficiently high energies. For the excitation processes examined in this paper, the Glauber total cross sections become essentially indistinguishable from the FBA at incident energies $E_i > 200$ eV. [redacted] Moreover, the derivation[1] of the formula (1) explicitly assumes that $\vec{q}$ is very nearly perpendicular to $\vec{K}_i$; this assumption also is specifically employed in the reduction of (1) to useable form (see section 3).

In excitation from state i to state f, the differential cross section is

$$\frac{d\sigma_{fi}}{d\Omega} = \frac{K_f}{K_i} |F_{fi}(\vec{q})|^2 \qquad (4)$$

and the total cross section is

$$\sigma_{fi}=\int\frac{K_f}{K_i}\ |F_{fi}(\vec{q})|^2\ \sin\theta d\theta d\phi \qquad (5)$$

where θ,ϕ are the angles in spherical coordinates specifying the direction of $\vec{K}_f$ relative to $\vec{K}_i$. Even in e-H(1s) collisions, the quantity $F_{fi}(\vec{q})$ need not be independent of ϕ, i.e., need not be axially symmetric about the z-axis, when u_f denotes a final state of specified magnetic quantum number, as e.g., in the 1s-2p excitation of hydrogen; of course, the differential cross section summed over final magnetic quantum numbers is independent of ϕ.

The quantity K_f is fixed by

$$\frac{\hbar^2}{2m}K_f^{\,2} + \varepsilon_f = \frac{\hbar^2}{2m}K_i^{\,2} + \varepsilon_i \qquad (6a)$$

where $\varepsilon_i,\varepsilon_f$ are the energies of the initial and final atomic states (with $\varepsilon_i = -13.6$ eV in the reactions we discuss). Thus from

$$q^2 = K_i^{\,2} + K_f^{\,2} - 2K_iK_f\cos\theta \quad , \qquad (6b)$$

$$qdq = K_iK_f\sin\theta d\theta$$

we can recast Eq. (5) into the form

$$\sigma_{fi} = \frac{1}{K_i^{\,2}}\int_{K_i-K_f}^{K_i+K_f} dq\ q\int_0^{2\pi} d\phi\ |F_{fi}(\vec{q})|^2 \qquad (7)$$

3. Cross Section Expressions

The desired expressions for inelastic 1s - 2s, 1s - 2p, 1s - 3s and 1s - 3p excitation of atomic hydrogen by electrons now can be obtained from Eqs. (1), (4) and (7), along with the appropriate initial and final wave functions. The immediately following subsection details the reduction of the integral (1) to usable form in the 1s - 2s case. As will be seen, the analysis closely parallels the previously reported[3] reduction of (1) in elastic e-H scattering.

3.1 1s - 2s Excitation

Introducing now atomic units, for 1s - 2s excitation

$$F_{fi}(\vec{q}) = \frac{iK_i}{2\pi}\int \frac{1}{4\pi\sqrt{2}}\,(2 - r)\; e^{-3r/2}\left[1 - \left(\frac{|\vec{b} - \vec{s}|}{b}\right)^{2in}\right] e^{i\vec{q}\cdot\vec{b}}\,(bdbd\phi_b)(sdsd\phi_s dz) \qquad (8)$$

where, because $\vec{q}$ is assumed to lie in the x,y plane containing $\vec{b}$ and $\vec{s}$ (see Fig. 1),

$$\vec{q}\cdot\vec{b} = qb\cos(\phi_b - \phi_q) \qquad (9)$$

$$|\vec{b} - \vec{s}| = \left[b^2 + s^2 - 2bs\cos(\phi_s - \phi_b)\right]^{1/2}$$

and of course

$r = (s^2 + z^2)^{1/2}$. Moreover, for given $\vec{K}_f$, i.e., for a given direction of scattering specified by given θ,ϕ in Eq. (5), then as we have defined $\vec{q}$

$$\phi_q = \phi + \pi$$

The expression (8) can be rewritten in the form

$$F_{fi}(\vec{q}) = \left\{ \left[2 + \frac{\partial}{\partial \lambda} \right] I_1(\vec{q}, \lambda) \right\}_{\lambda = 3/2} \tag{10}$$

where

$$I_1(\vec{q}, \lambda) = \frac{i K_i}{8\pi^2 \sqrt{2}} \int e^{-\lambda r} \left[1 - \left(\frac{|\vec{b} - \vec{s}|}{b} \right)^{2in} \right] e^{i \vec{q} \cdot \vec{b}} (b\,db\,d\phi_b)(s\,ds\,d\phi_s\,dz) \tag{11}$$

Now, because of (9) and using $Y = 2b_s/(b^2 + s^2)$,

we obtain,

$$I_1 = \frac{i K_i}{8\pi^2 \sqrt{2}} \int e^{-\lambda r} \left[2\pi - \left(\frac{2s}{bY} \right)^{in} \int_0^{2\pi} d\phi_s \, (1 - Y \cos\phi_s)^{in} \right] e^{i \vec{q} \cdot \vec{b}} (b\,db\,d\phi_b) \times (s\,ds\,dz) \tag{12}$$

$$= \frac{i K_i}{4\pi \sqrt{2}} \int_0^\infty db \int_0^\infty ds \int_{-\infty}^\infty dz \; b\,s\, e^{-\lambda (s^2 + z^2)^{1/2}} J_0(qb) \left[2\pi - \left(\frac{2s}{bY} \right)^{in} \int_0^{2\pi} d\phi_s (1 - Y \cos\phi_s)^{in} \right] \tag{13}$$

$$= \frac{i K_i}{2\pi \sqrt{2}} \int_0^\infty db \int_0^\infty ds \; s^2 b \, K_1(\lambda s) J_0(qb) \left[2\pi - \left(\frac{2s}{bY} \right)^{in} \int_0^{2\pi} d\phi_s \, (1 - Y \cos\phi_s)^{in} \right] \tag{14}$$

The result (14) is obtained from (13) by, e.g., introducing the new integration variable

τ instead of z via $z = a \sinh \tau$, and them employing a standard formula[8] for K_ν, the modified Bessel function of the third kind.

The integral (14) is further reduced by transforming to polar coordinates in the b,s plane,

$$S = R \sin\theta'$$

$$b = R \cos\theta'$$

This transformation makes y and s/bY in (14) independent of R, so that we can use[9]

$$\int_0^\infty dR\, R^4 K_1(\lambda R \sin\theta') J_0(qR\cos\theta') = \frac{2^4}{(\lambda\sin\theta')^5}\, {}_2F_1\left(3, 2; 1; -\frac{q^2}{\lambda^2}\cot^2\theta'\right) \qquad (15)$$

Furthermore[10]

$${}_2F_1\left(3, 2; 1; -\frac{q^2}{\lambda^2}\cot^2\theta'\right) = \left(1 + \frac{q^2}{\lambda^2}\cot^2\theta'\right)^{-4} {}_2F_1\left(-2, -1; 1; -\frac{q^2}{\lambda^2}\cot^2\theta'\right)$$

$$= \left(1 + \frac{q^2}{\lambda^2}\cot^2\theta'\right)^{-4}\left(1 - \frac{2q^2}{\lambda^2}\cot^2\theta'\right) \qquad (16)$$

Therefore,

$$I_1 = \frac{16 i K_i}{\sqrt{2}} \int_0^{\pi/2} \frac{d\theta' \sin^2\theta' \cos\theta'}{(\lambda\sin\theta')^5}\left(1 + \frac{q^2}{\lambda^2}\cot^2\theta'\right)^{-4}\left(1 - \frac{2q^2}{\lambda^2}\cot^2\theta'\right)$$

$$\times\left[1 - \frac{1}{2\pi}\left(\frac{1}{\cos\theta'}\right)^{2in} \int_0^{2\pi} d\phi_s\, (1 - \sin 2\theta' \cos\phi_s)^{in}\right] \qquad (17)$$

From Eqs. (10) and (17), after setting $\lambda = 3/2$,

$$F_{fi}(\vec{q}) = \frac{2^{10} k K_i}{3^6 \sqrt{2}} \int_0^{\pi/2} d\theta' \frac{\sin^3\theta' \cos\theta'}{(\sin^2\theta' + \frac{4}{9} q^2 \cos^2\theta')^5} \left\{ \left[-2\sin^4\theta' + \frac{56}{9} q^2 \cos^2\theta' \sin^2\theta' - \frac{128}{81} q^4 \cos^4\theta' \right] \cdot \left[1 - \frac{1}{2\pi} \left(\frac{1}{\cos\theta'} \right)^{2in} \int_0^{2\pi} d\phi_s (1 - \sin 2\theta' \cos\phi_s)^{in} \right] \right\} \tag{18}$$

Eq. (18) shows $F_{fi}(\vec{q})$ is independent of scattering azimuth angle ϕ, as it should be in the present case of 1s - 2s excitation. We have evaluated $F_{fi}(\vec{q})$ numerically from Eq. (18) by two independent methods, which have yielded essentially identical results. Our first method involves computing the integral over ϕ_s numerically, after which we perform the second numerical integration over θ' (but, for convenience, first replacing θ' by the new integration variable t via $t = \sin\theta'$). In our second method we have evaluated the integral over ϕ_s in (18) from the previously used[13] formula

$$\frac{1}{2\pi} \int_0^{2\pi} d\phi_s (1 - \sin 2\theta' \cos\phi_s)^{in} = |\cos 2\theta'|^{2in+1} {}_2F_1\left(\frac{in}{2} + \frac{1}{2}, \frac{in}{2} + 1; 1; \sin^2 2\theta' \right) \tag{19}$$

Eq. (19) can be derived, e.g., by writing (when, as in (18), $0 < \theta' < \pi/2$)

$$1 - \sin 2\theta' \cos\phi_s = |\cos 2\theta'| \left[|\sec 2\theta'| - |\tan 2\theta'| \cos\phi_s \right]$$

and then using a known integral representation[11] for the Legendre function, which is expressible[12] in terms of the hypergeometric function ${}_2F_1$.

To convert to c.g.s. units, replace K_i and q in (18) by $a_o K_i'$ and $a_o q'$, where the primed quantities are in c.g.s. units (i.e., $K_i' = mv_i/\hbar$ in c.g.s. units), and multiply the right side of (18) by an extra factor a_o, consistent with F_{fi} having the dimensions of length.

3.2 1s - 3s Excitation

In atomic units, after introducing the 1s and 3s wave functions, Eq. (1) becomes

$$F_{fi}(\vec{q}) = \frac{iK_i}{2\pi}\int \frac{1}{81\pi\sqrt{3}}\left(27 + 18\frac{\partial}{\partial\lambda} + 2\frac{\partial^2}{\partial\lambda^2}\right) e^{-\lambda r}\left[1 - \left(\frac{|\vec{b}-\vec{s}|}{b}\right)^{2in}\right]$$

$$\times e^{i\vec{q}\cdot\vec{b}}\,(b\,db\,d\phi_b)(s\,ds\,d\phi_s\,dz) \qquad (20)$$

evaluated at $\lambda = 4/3$. Recalling Eqs. (11) and (17), one finds Eq. (20) reduces to

$$F_{fi}(\vec{q}) = \frac{81}{64}\frac{iK_i}{\sqrt{3}}\int_0^{\pi/2} d\theta' \frac{\sin^3\theta'\cos\theta'}{(\sin^2\theta' + \frac{9}{16}q^2\cos^2\theta')^6}\left\{\left[-\sin^6\theta' - \frac{9}{8}q^2\sin^4\theta'\cos^2\theta'\right.\right.$$

$$\left. + \frac{3^7}{2^8}q^4\sin^2\theta'\cos^4\theta' - \frac{3^7}{2^{10}}q^6\cos^6\theta'\right]$$

$$\left.\times\left[1 - \frac{1}{2\pi}\left(\frac{1}{\cos\theta'}\right)^{2in}\int_0^{2\pi} d\phi_s\,(1 - \sin 2\theta'\cos\phi_s)^{in}\right]\right\} \qquad (21)$$

3.3 1s - 2p Excitation

The observed 1s - 2p excitation cross section is the sum of the cross sections for excitation to each of the 2p magnetic substates. For our present purposes, the electron spin, $2p_{1/2} - 2p_{3/2}$ splitting and hyperfine effects all are inconsequential, so that the electrons can be considered spinless in effect, and the 2p magnetic substates can be labeled merely by the orbital magnetic quantum numbers m = 0, ± 1. Let the direction of $\vec{K}_i$ (the z-axis employed in section 2) be the axis of quantization for the atomic wave functions. Then for excitation to m = 0, Eq. (1) yields

$$F_{fi}(\vec{q}) = \frac{iK_i}{2\pi}\int \frac{1}{4\pi\sqrt{2}}\, r e^{-\lambda r}\cos\theta_s \left[1 - \left(\frac{|\vec{b}-\vec{s}|}{b}\right)^{2.14}\right] e^{i\vec{q}\cdot\vec{b}}\,(b\,db\,d\phi_b)(s\,ds\,d\phi_s\,dz) \qquad (22)$$

where $z = r\cos\theta_s$ and $\lambda = 3/2$. Thus $F_{fi}(\vec{q})$ from (22) vanishes, since it is integrated from $z = -\infty$ to $+\infty$ and the integrand is an odd function of z. It can be seen that this result--namely that $F_{fi}(\vec{q})$ vanishes for excitation to the 2p m = 0 state--is a consequence of the Glauber theory assumption that $\vec{q}$ is perpendicular to $\vec{K}_i$. In FBA, where one does not assume $\vec{q} \perp \vec{K}_i$, the 1s - 2p m = 0 excitation amplitude is not identically zero. However, examination of the quite complicated closed form FBA expressions[13] for the 1s - 2p m = 0, ± 1 amplitudes indicates that (for those scattering angles making the predominant contribution to the excitation cross sections) the m = 0 amplitude becomes negligible compared to the m = ± 1 amplitudes in the limit $E_i \to \infty$. This conclusion concerning the high energy behavior of the FBA 1s - 2p m = 0, ± 1 amplitudes is supported by numerical calculations[14], which show that the FBA 1s - 2p m = 0 integrated cross section decreases

much more rapidly than the FBA 1s - 2p m = ± 1 integrated cross sections as the energy increases from 13 eV to 200 eV. Thus the Glauber result that the 1s - 2p m = 0 amplitude vanishes is not inconsistent with the expectation (explained in section 2) that the Glauber total cross section predictions should merge with the FBA at large E_i. We stress that the preceding sentence pertains to quantization along $\vec{K}_i$ only. In FBA it is more usual and more convenient to quantize along $\vec{q}$, in which event the FBA 1s - 2p m = ± 1 amplitudes vanish, and the dominant FBA amplitude is the 1s - 2p m = 0.

For 1s - 2p excitation to m = 1,

$$F_{fi}(\vec{q}) = \frac{iK_i}{2\pi}\int \frac{1}{8\pi} r e^{-\lambda r} \sin\theta_s e^{i\phi_s}\left[1 - \left(\frac{|\vec{b}-\vec{s}|}{b}\right)^{2in}\right] e^{i\vec{q}\cdot\vec{b}} (b\,db\,d\phi_b)(s\,ds\,d\phi_s\,dz) \tag{23}$$

with λ again = 3/2. But $r\sin\theta_s = s$. So (23) can be rewritten as

$$F_{fi}(\vec{q}) = \frac{iK_i}{16\pi^2}\int ds\,db\,dz\; bs^2 e^{-\lambda(s^2+z^2)^{1/2}} e^{i\phi_q}\int d\phi_b\, e^{i(\phi_b-\phi_q)} e^{i\vec{q}\cdot\vec{b}} \times \int d\phi_s\, e^{i(\phi_s-\phi_b)}\left[1 - \left(\frac{|\vec{b}-\vec{s}|}{b}\right)^{2in}\right] \tag{24}$$

Recalling (9), in (24)

$$\int_0^{2\pi} d\phi_s\, e^{i(\phi_s-\phi_b)}\left[1 - \left(\frac{|\vec{b}-\vec{s}|}{b}\right)^{2in}\right] = -\left(\frac{2s}{bY}\right)^{in}\int_0^{2\pi} d\phi_s \cos\phi_s (1 - Y\cos\phi_s)^{in} \tag{25}$$

where Y is as in Eq. (12). Thus

$$F_{fi}(\vec{q}) = \frac{K_i e^{i\phi_q}}{8\pi}\int ds\,db\,dz\; bs^2 e^{-\lambda(s^2+z^2)^{1/2}} J_1(qb)\left(\frac{2s}{bY}\right)^{in}\int_0^{2\pi}\cos\phi_s(1-Y\cos\phi_s)^{in}d\phi_s \tag{26}$$

$$= \frac{K_i e^{i\phi_q}}{4\pi}\int ds\,db\; bs^3 K_1(\lambda s) J_1(qb)\left(\frac{2s}{bY}\right)^{in}\int_0^{2\pi} d\phi_s \cos\phi_s(1-Y\cos\phi_s)^{in} \tag{27}$$

As in subsection 3.1, introducing polar coordinates in the b,s plane, Eq. (27) reduces to

$$F_{fi}(\vec{q}) = \frac{2^{12} K_i}{3^6 \pi} q\, e^{i\phi_q} \int_0^{\pi/2} \frac{d\theta' \cos^2\theta' \sin^4\theta' \left[\sin^2\theta' - \frac{4}{9} q^2 \cos^2\theta'\right] \left(\frac{1}{\cos\theta'}\right)^{2in}}{\left(\sin^2\theta' + \frac{4}{9} q^2 \cos^2\theta'\right)^5} \int_0^{\pi} d\phi_s \cos\phi_s (1 - \gamma\cos\phi_s)^{in} \tag{28}$$

where $Y = \sin 2\theta'$. We have computed $F_{fi}(\vec{q})$ numerically from (28), after introducing the new integration variable $t = \sin\theta'$. Note that $F_{fi}(\vec{q})$ now depends on the scattering azimuth angle $\phi = \phi_q - \pi$, as foreshadowed in section 2. However, $|F_{fi}(\vec{q})|^2$ remains independent of ϕ. The quantity $|F_{fi}(\vec{q})|^2$ for 1s - 2p m = - 1 obviously is the same as for m = 1.

In (28), the integral over ϕ_s also can be expressed as a hypergeometric function. Using (19) and the properties[15] of the derivative of ${}_2F_1$,

$$\int_0^{\pi} d\phi_s \cos\phi_s \,(1 - Y\cos\phi_s)^{in} = -\tfrac{1}{2}(in+1)^{-1} \frac{\partial}{\partial Y} \int_0^{2\pi} d\phi_s \,(1 - Y\cos\phi_s)^{in+1}$$

$$= -\frac{\pi}{in+1} \frac{\partial}{\partial Y} \left[(1-Y^2)^{in+\frac{3}{2}}\; {}_2F_1\left(\tfrac{in}{2}+1, \tfrac{in}{2}+\tfrac{3}{2}; 1; Y^2\right)\right]$$

$$= -\frac{in\pi Y}{2} (1-Y^2)^{in+\frac{1}{2}}\; {}_2F_1\left(\tfrac{in}{2}+1, \tfrac{in}{2}+\tfrac{3}{2}, 2; Y^2\right)$$

3.4 1s - 3p Excitation

As in subsection 3.3, the 1s - 3p m = 0 amplitude vanishes; also, the values of $|F_{fi}(\vec{q})|^2$ for m = ± 1 are equal and independent of ϕ. For 1s - 3p m = 1, we find

$$F_{fi}(\vec{q}) = \frac{2^8 K_i q e^{i\phi_q}}{27\pi} \int_0^{\pi/2} \frac{d\theta' \cos^2\theta' \sin^4\theta'}{(\lambda^2 \sin^2\theta' + q^2\cos^2\theta')^6} \left\{ \left[\lambda^4 (6\lambda - 7) \sin^4\theta' + 12\lambda^2 q^2 \sin^2\theta' \cos^2\theta' \right.\right.$$

$$\left.\left. -(6\lambda+1) q^4 \cos^4\theta' \right] \frac{1}{(\cos^2\theta')^{in}} \int_0^{\pi} d\phi_s \cos\phi_s \left(1 - \sin 2\theta' \cos\phi_s\right)^{in} \right\} \tag{29}$$

evaluated at $\lambda = 4/3$.

4. Results and Discussion

In the immediately following subsection, we concentrate on the total cross section for 1s - 2s excitation. Subsequent subsections discuss $\sigma_{2p,1s}$; present the computed $\sigma_{3s,1s}$ and $\sigma_{3p,1s}$; and examine the predicted differential cross sections. Conclusions concerning the validity and utility of Glauber theory for computing excitation cross sections in electron-atom collisions, as evidenced by the results of this paper, are summarized in the final subsection 4.5.

4.1 Total 1s - 2s Cross Section

Figure 2 compares our Glauber total 1s - 2s excitation cross sections with a variety of previous theoretical estimates of $\sigma_{2s,1s}$. Specifically, Fig. 2 plots $\sigma_{2s,1s}$ vs. E_i as computed via FBA[16] (curve 1); second Born

approximation[17], in which however contributions from coupling to highly excited (principal quantum number n > 5) intermediate states have been estimated only approximately, using closure (curve 6); distorted wave approximation[18] (curve 7); a 1s - 2s - 2p close coupling calculation, including exchange[19] (curve 5); FBA combined with the Ochkur approximation[20] for the exchange amplitude (curve 2); the so-called Vainshtein approximation[7] (curve 3); and finally the Glauber (curve 4). It is seen that all methods give essentially the same results above 200 eV, and that significant differences between the various approximations do not set in until the incident energy is decreased below 100 eV. We note that the Glauber predictions tend to lie below the others, especially at energies < 30 eV. In particular, the Glauber $\sigma_{2s,1s}$ is well below the FBA at energies < 100 eV; this behavior of the Glauber excitation cross section $\sigma_{2s,1s}$ contrasts with the behavior of the Glauber elastic $\sigma_{1s,1s}$, which exceeds the FBA $\sigma_{1s,1s}$ at all energies[3].

Figure 3 compares the experimentally observed 1s - 2s excitation cross sections with the Glauber predictions (solid curve). The solid circle data points are from the very recent measurements of Kauppila, Ott and Fite[21]. The agreement between these observations and the Glauber theoretical values is quite good in the energy range above 30 eV. Referring to Fig. 2, it can be seen that--except for the Vainshtein--the Glauber is the only theoretical estimate which will be reasonably close to the data of Kauppila et al. in the energy range 30 eV to 100 eV; all other theories predict $\sigma_{2s,1s}$ cross sections which are much too high, e.g., the FBA (dashed curve in Fig. 3). Moreover, it is fair to say that the Vainshtein approximation rests on a very uncertain theoretical foundation[22], in that calculations via this method incorporate subsidiary physically unjustified mathematical simplifications (e.g.,

a so-called peaking approximation) introduced solely for the purpose of making integrals tractable.

We also remark that although the magnitudes of the experimental cross sections have been in dispute for some years[21,23], it seems unlikely that future experiments will yield observed $\sigma_{2s,1s}$ much larger than observed by Kauppila et al.[21], i.e., it seems unlikely that future experiments will cause the Glauber to look poorer than, e.g., the 1s - 2s - 2p close coupling (curve 5 of Fig. 2) in 30 eV < E_i < 100 eV. The very careful experiments of Kauppila et al. assume that $\sigma_{2p,1s}$ is correctly given by FBA at 200 eV, which is a perfectly reasonable assumption, judging by Fig. 4 below. Actually their results show that Kauppila et al. equally well could have normalized their inferred $\sigma_{2s,1s}$ to the Born approximation $\sigma_{2s,1s}$ at 200 eV, which energy should be high enough for the FBA $\sigma_{2s,1s}$ to be reliable, judging now by Fig. 2. Moreover, the results of Kauppila et al. lie above those reported by Hils, Kleinpoppen and Koschmieder[24], who normalized to FBA at the even higher energy of 500 eV. At very low energies, E_i < 40 eV, there are $\sigma_{2s,1s}$ data by Lichten and Schulz[25] which originally were reported to lie considerably higher than the Kauppila et al. points of Fig. 3, but which were based on normalization to FBA at 40 eV, which clearly is too low an energy to rely on FBA. When the Lichten and Schulz data at 25 eV are renormalized so that they coincide with Kauppila et al. at 25 eV (which in effect renormalizes the Lichten and Schulz data to FBA at 200 eV), the Lichten-Schulz and Kauppila cross sections are in quite good agreement[21] over the entire energy range E_i < 40 eV wherein the two experiments overlap.

Another remark worth making is that in the very low energy range 10.2 eV < E_i < 13 eV, six state 1s - 2s - 2p - 3s - 3p - 3d close coupling

calculations (including exchange) have been carried out[26], whose results are quite close[21] to the Lichten and Schulz data renormalized as described in the preceding paragraph. Furthermore, this inclusion of coupling to n = 3 states significantly decreases[26] the predicted $\sigma_{2s,1s}$ from their three state 1s - 2s - 2p close coupling values (curve 5 of Fig. 2). It is possible, therefore, that a six state close coupling calculation would satisfactorily agree with the Kauppila data points of Fig. 3, perhaps even over the entire range 10.2 eV < E_i < 200 eV. At the present time this possibility cannot be verified however; because the computations are so tedious, no six state close coupling calculations of $\sigma_{2s,1s}$ at energies E_i > 13 eV have been carried out. Thus for close coupling predictions at E_i > 13 eV one is forced to fall back on the obviously inadequate (for energies 13 < E_i < 100 eV) three state 1s - 2s - 2p results[19]. Actually, the success of the Glauber in Fig. 2--if not fortuitous--suggests that the close coupling method is much more elaborate than necessary, for predicting $\sigma_{2s,1s}$ in the energy range E_i > 30 eV at any rate; certainly the Glauber diffraction approximation ignores the interchannel coupling (supposedly capable of causing many successive excitations and deexcitations during the incident electron's transit of the target hydrogen atom) whose inclusion so greatly complicates the close coupling computations.

As explained in section 2, the Glauber curve of Fig. 3 perforce neglects electron exchange. Therefore the Glauber theory's apparent success for $\sigma_{2s,1s}$ excitation indeed would be fortuitous if neglect of exchange were unjustified above 30 eV. Various theoretical calculations[27] indicate that exchange should be quite negligible at incident energies E_i > 100 eV, but may become fairly important at E_i < 50 eV. Unfortunately, there are no very reliable means of quantitatively determining exchange contributions to cross sections at those low energies where exchange is likely to be non-negligible.

However, we have employed the Born-Oppenheimer (B-0) approximation[27] to estimate the exchange amplitude in 1s - 2s excitation. In this 1s - 2s case, including the B-0 exchange amplitude along with the Glauber direct amplitude alters the solely Glauber predictions by only a few percent for 40 eV < E_i < 70 eV and all consequential scattering angles (angles making non-negligible contributions to the integrated cross section); above 100 eV the exchange contribution estimated in B-0 is utterly negligible, as far as the integrated cross section is concerned. Similar comments pertain to use of the Ochkur approximation for the exchange amplitude[20]. Below 40 eV the B-0 exchange amplitude becomes more important compared to the Glauber direct amplitude, but in this energy range the B-0 amplitude tends to overestimate the exchange contribution, as is well known[27]. We conclude that neglect of exchange in the Glauber curve of Fig. 3 is justified in the energy range E_i > 30 eV where the Glauber fits the data of Kauppila et al. Neglect of exchange may be a reason (though not the sole possible reason, see subsection 4.5 below) for the apparent failure of the Glauber theory at E_i < 30 eV in Fig. 3.

The measurements plotted in Fig. 3 do not distinguish between H(2s) atoms created by 1s - 2s excitation, and those produced by radiative cascading to H(2s) after excitation to higher levels, e.g., H(4p). Therefore the effective $\sigma_{2s,1s}$ observed in the experiments quoted in Fig. 3 must be

$$\sigma^{eff}_{2S,1S} = \sigma_{2S,1S} + \sum_j P(j \to 2S)\, \sigma_{j,1S} \qquad (30)$$

summed over all energetically accessible levels j lying above H(2s), with P(j → 2s) the probability of cascading to H(2s) after initial excitation to H(j). The predominant cascade mechanism to H(2s) is via excitation to H(3p), i.e., the largest term in the above sum corresponds to j = 3p. Thus it is

customary to rewrite (30) in the more convenient form

$$\sigma^{\#\#}_{2s,1s} = \sigma_{2s,1s} + \gamma \sigma_{3p,1s} \qquad (31)$$

where γ is computable from known transition probabilities[28] combined with estimates of the ratios $\sigma_{j,1s}/\sigma_{3p,1s}$. It seems to be generally agreed[21,24], on the basis of Hummer and Seaton's[29] FBA estimates of these ratios, that $\gamma = 0.23$ over a broad range of energies. Consequently the theoretical curves in Fig. 3 are plots of the right side of (31), using $\gamma = 0.23$. To be quite specific, in the dashed curve of Fig. 3 we use the FBA values of $\sigma_{2s,1s}$ and $\sigma_{3p,1s}$; in the solid Glauber curve we use $\sigma_{2s,1s}$ from Fig. 2 and the Glauber $\sigma_{3p,1s}$ from Fig. 6 below.

Actually, we have recomputed γ, using a somewhat more extensive set[16] of computed FBA cross sections than was available to Hummer and Seaton[29]. We find γ indeed is very nearly constant over the energy range of interest in Fig. 3, but that $\gamma = 0.19$ rather than 0.23. Use of this smaller value of γ makes the agreement between the Glauber theory and the Kauppila data even better than is shown in Fig. 3; however, because we have no prior assurance that the Glauber predicted $\sigma_{2s,1s}$ and $\sigma_{3p,1s}$ are very accurate at $E_i > 30$ eV, we do not wish to conclude that $\gamma = 0.19$ is nearer the truth than $\gamma = 0.23$ when the exact $\sigma_{2s,1s}$ and $\sigma_{3p,1s}$ are used in Eq. (31). We add that if (as we claim) Glauber theory really is much superior to FBA, then the ratios $\sigma_{j,1s}/\sigma_{3p,1s}$ used to compute γ should be estimated from Glauber calculations, not from FBA. After $j = 3p$, the most important contributors (in FBA) to the sum in (30) are the $j = np$ terms, $n > 3$. We have not computed the Glauber $\sigma_{np,1s}$ for $n > 3$, so that we cannot immediately test the validity of the FBA

estimated $\sigma_{np,1s}/\sigma_{3p,1s}$ for n > 3. But our computations do enable us to compare the FBA and Glauber ratios $\sigma_{3p,1s}/\sigma_{2p,1s}$. We find that these ratios are very nearly equal at energies E_i > 30 eV. Therefore, for energies exceeding 30 eV at any rate, estimates of γ in (31) from the FBA ratios $\sigma_{j/1s}/\sigma_{3p,1s}$ should be quite accurate.

4.2 Total 1s - 2p Cross Sections

In Fig. 4 we compare theoretical and experimental values of the total 1s - 2p excitation cross section. The sources and descriptions of the theoretical curves in Fig. 4 are the same as those cited in connection with Fig. 2 above, e.g., curve 6 in Fig. 4 is the Holt and Moiseiwitsch[17] second Born approximation for $\sigma_{2p,1s}$, in which however contributions to highly excited (n > 5) intermediate states have been estimated only approximately, using closure. As in the 1s - 2s case, all theories are fairly close for E_i > 100 eV; for E_i < 100 eV the Glauber tends to be significantly lower than other theoretical calculations, excepting the Vainshtein (curve 3). The triangles in Fig. 4 are the experimental data points of Long, Cox and Smith[30], which are the most recent measurements of $\sigma_{2p,1s}$, and which are in good agreement with older experiments[31,32]. Because cascading is estimated[30] to make only a two percent contribution to the observed $\sigma_{2p,1s}$, in Fig. 4 it is legitimate to compare the observed data points with theoretical curves uncorrected for cascading (as would not have been legitimate in Fig. 2). Again we see that the Glauber theory is in good agreement with experiment at energies E_i > 30 eV, but is rather lower than observed for E_i < 30 eV. In particular, at energies 30 eV < E_i < 100 eV, the Glauber is distinctly superior to all other theoretical calculations shown in Fig. 4, excluding the not well-founded Vainshtein.

Actually, the data points shown in Fig. 4 have had to be computed from the values reported by Long et al.[30], because those observers--as well as previous workers[31,32]--only measure $Q_\perp$, defined as 4π times the number of Lyman alpha photons per unit solid angle emitted in a direction perpendicular to the direction of the incident electron beam, normalized at 200 eV to the number expected from FBA. The total cross section σ to be plotted in Fig. 4 is given in terms of $Q_\perp$ by[33]

$$\sigma = \frac{3 - P}{3} Q_\perp \tag{32}$$

where the polarization fraction P has its customary definition

$$P = \frac{I_\parallel - I_\perp}{I_\parallel + I_\perp} \tag{33}$$

in terms of the intensities, observed at 90° to the electron beam axis, of the Lyman α components having electron vectors parallel and perpendicular to the electron beam axis. Values of $P(E_i)$ have been measured recently by Ott, Kauppila and Fite[33]. Using these values in (32), together with the normalized $Q_\perp(E_i)$ reported by Long et al., yields the data points plotted in Fig. 4.

Recently there has been much interest in the Gryzinski[34] classical model for prediction of atomic collision cross sections. The Gryzinski predictions have the virtue that they are extremely easy to compute, even easier than the FBA and the Glauber. However, the Gryzinski prescription[34] for computing excitation cross sections yields only the total cross section for excitation to the n = 2 levels of atomic hydrogen; the Gryzinski formulation does not distinguish between excitation to degenerate (or nearly degenerate) levels of different orbital angular momentum. For this reason,

in Fig. 5 we have plotted theoretical and experimental values of the total cross section for excitation to the hydrogen n = 2 levels. The solid curve is the sum of the Glauber curves (curves 4) in Figs. 2 and 4; the dashed curve is the similar sum of the FBA curves (curves 1) in Figs. 2 and 4; the dot-dashed curve is the Gryzinski prediction, as computed by Stabler[35]. The triangles in Fig. 5 are the data, obtained by adding the solid circles in Fig. 3 to the triangles in Fig. 4. Evidently the Glauber is a much better fit than the Gryzinski; however, the trivial Gryzinski computation does correctly predict the peak combined cross section ($\sigma_{2s,1s} + \sigma_{2p,1s}$) to within 50%. We note that in adding the experimental points of Figs. 3 and 4 we are including the contribution from cascading to H(2s), which contribution is not included in the theoretical curves of Fig. 5. On the other hand, the experimental points in Fig. 3 lie much lower than those in Fig. 4, i.e., the experimental (and theoretical) curves in Fig. 5 are dominated by $\sigma_{2p,1s}$; consequently, subtraction of the cascading contribution to the experimentally observed H(2s) production would only slightly modify the experimental points of Fig. 5.

4.3 Total 1s - 3s and 1s - 3p Cross Sections

In Fig. 6 are displayed the Glauber predictions for $\sigma_{3s,1s}$ and $\sigma_{3p,1s}$ (solid curves), together with FBA[16] (short dashes) and distorted wave[18] (long dashes) calculations; in addition, for 1s - 3p excitation only, there are shown results computed in a two state 1s - 3p close coupling approximation[19], including exchange. There are no reliable data with which these predictions can be compared. The relations between the various curves in Fig. 6 are much the same as was found for the corresponding curves of Figs. 2 and 4.

4.4 Differential Cross Sections

As yet we have not discussed differential cross section predictions; these are shown in Fig. 7, for excitation to 2s, 2p, 3s and 3p at an incident electron energy of 100 eV. In Fig. 7, the solid curves are the Glauber results; the dashed curves are FBA differential cross sections, taken from Mott and Massey[36]. The absolute differential cross sections are plotted in Fig. 7, with the scale on the left referring to the 1s - 2s and 1s - 3s curves, while the scale on the right pertains to the 1s - 2p and 1s - 3p curves. The scales in Fig. 7 are much more condensed than those employed in Figs. 2, 4 and 6, so that, e.g., the differences between the FBA and Glauber 1s - 2p curves in Fig. 7 do account for the roughly 10% difference between the FBA nd Glauber total $\sigma_{2p,1s}$ curves of Fig. 4 at 100 eV.

As in e - H elastic scattering[3,4], the Glauber and FBA curves of Fig. 7 all decrease monotomically with increasing scattering angle θ. In a number of other respects, however, the relations between corresponding Glauber and FBA curves of Fig. 7 are rather different than was the case for elastic scattering. At large angles, $\theta > \sim 40^{\circ}$, the Glauber inelastic differential cross sections are significantly larger than the FBA; in elastic scattering at large angles the FBA and Glauber were practically indistinguishable[3,4], but if anything the FBA exceeded the Glauber. In elastic scattering at angles $0^{\circ} < \theta < \sim 40^{\circ}$, the Glauber always exceeded the FBA, with the difference between the FBA and Glauber becoming quite large at very small angles $\theta < \sim 10^{\circ}$; as a result, the Glauber total elastic cross section $\sigma_{1s,1s}$ exceeded[3] the FBA $\sigma_{1s,1s}$. On the other hand, in the 100 eV differential cross sections of Fig. 7, the Glauber 1s - 2s curve only slightly exceeds the FBA 1s - 2s in the angular range $\theta < 10^{\circ}$, while at intermediate angles $10^{\circ} < \theta < 40^{\circ}$ the

Glauber 1s - 2s lies significantly below the FBA; consequently, recalling that in computing the total cross section the differential cross section $d\sigma/d\Omega$ is weighted by an extra factor sin θ, it is understandable that the Glauber total inelastic $\sigma_{2s,1s}$ turns out to be less than the FBA $\sigma_{2s,1s}$ at 100 eV, as was shown in Fig. 2. In the 1s - 3s case, the Glauber $d\sigma/d\Omega$ of Fig. 7 starts out only very slightly above the FBA at 0^o, and falls below the FBA at an angle θ as small as 2^o. The 1s - 2p and 1s - 3p Glauber curves of Fig. 7 lie below their corresponding FBA curves even at 0^o.

The features of the foregoing comparisons between Glauber and FBA inelastic differential cross sections are quite characteristic, i.e., these features appear to persist at essentially all energies 10 eV < E_i < 200 eV. In general the differences between the Glauber and FBA inelastic $d\sigma/d\Omega$ become more marked at consequential angles (angles contributing significantly to the integrated cross section) as the energy is decreased. To illustrate this remark, in Fig. 8 we plot $|F_{2s,1s}(\vec{q})|^2$ from Eq. (18), as a function of q^2, for incident energies of 50 eV, 100 eV and 200 eV (solid curves); for comparison the FBA $|F_{2s,1s}(\vec{q})|^2$, which is independent of incident energy, also is shown (dashed curve). For given E_i, $q^2(\theta)$ is a monotonically increasing function of scattering angle θ, but the value of q^2 at 0^o increases as the incident energy decreases, e.g., at E_i = 100 eV, $q^2(0^o)$ = 0.02, while at E_i = 50 eV, $q^2(0^o)$ = 0.04. Thus the fact that in Fig. 2 the FBA $\sigma_{2s,1s}$ lies increasingly above the Glauber $\sigma_{2s,1s}$ as the energy is decreased from 200 eV to about 20 eV also can be understood from Fig. 8, recalling that in computing the total cross section via Eq. (7) the quantity $|F_{fi}(\vec{q})|^2$ in the integrand is weighted by an extra factor q, while the lower integration limit is $[q^2(0^o)]^{\frac{1}{2}}$. Below about 20 eV the Glauber and FBA $\sigma_{2s,1s}$ again approach

Moreover, in the range $10^{-1} < q^2 < \sim 3$ the Glauber curves lie below the Born, the more so as E_i decreases.

each other in Fig. 2 because the integration range $K_i - K_f$ to $K_i + K_f$ in Eq. (7) rapidly diminishes as threshold $K_f = 0$ is approached.

The only angular distribution data with which our Glauber predictions can be compared are those of Williams[37], who has measured the angular distribution of those scattered electrons whose energy loss corresponds to excitation of the n = 2 levels of atomic hydrogen. Figure 9 shows Williams' data points (labeled 1) at an incident electron energy $E_i = 50$ eV, normalized at 20° to the sum of the cross sections for excitation of H(2s) and H(2p), as calculated (at 54 eV) by Scott[38] in the 1s - 2s - 2p close coupling approximation. Curves 2 and 3 in Fig. 9 also are taken directly from Williams[37]. Curve 2 shows the aforementioned 1s - 2s - 2p close coupling predictions[38]; curve 3 shows the Born-Oppenheimer (B-O) predictions (again at 54 eV), also normalized at 20° to the observations. As Williams remarks, at angles $\theta < \sim 80^\circ$ the B-O curve is essentially identical with the FBA. At angles $\theta > 80^\circ$ the effects of electron exchange cause the B-O curve to turn up; the FBA, which neglects exchange, continues to decrease monotonically as θ increases beyond 80°, consistent with our discussion of Fig. 7. Curve 4 of Fig. 9 displays the Glauber predictions, for $E_i = 50$ eV, normalized (like the other theoretical curves) to the data points at 20°. At angles $20^\circ < \theta < 40^\circ$ there is not much to choose between the various theories. For $\theta > 40^\circ$ the 1s - 2s - 2p close coupling gives a quite good fit, while the FBA or B-O are clearly bad fits. The Glauber is not quite as good as the 1s - 2s - 2p close coupling at $\theta > 40^\circ$, but the Glauber fit certainly is not poor. It will be recalled that the 1s - 2s - 2p close coupling calculations --although much more arduous than the Glauber--at 50 eV actually predicted much less accurate total $\sigma_{2s,1s}$ and $\sigma_{2p,1s}$ than did the Glauber (Figs. 2 - 4).

Figure 10 compares Williams' data[37] (curves 1) with theoretical angular distributions at incident electron energies of 100 eV (Fig. 10a) and 200 eV (Fig. 10b). At these energies there are no close coupling calculations, so Williams fitted his observations to the B-O (curves 2) at 21^{o}. As was the case at 50 eV, these 100 eV and 200 eV B-O curves are bad fits to the observed points. In addition, Fig. 10 shows the Glauber predictions (curves 3), also normalized to Williams' data points at 21^{o}. At 100 eV the Glauber again is an acceptable fit; at 200 eV the Glauber fit is excellent. It is noteworthy that at fixed large angle (e.g., $\theta = 60^{o}$) the deviation between the Glauber and the FBA increases with increasing energy in Figs. 9 - 10, contrary to the (now seen to be dubious) inference in section 2 that the Glauber $F_{fi}(\vec{q})$ should approach the Born $F_{fi}(\vec{q})$ at high energies. We add that except at backward angles, where the B-O amplitudes approach the Glauber, inclusion of electron exchange could not significantly modify any of the Glauber curves in Figs. 9 - 10.

Of course, 200 eV is not really a high enough energy to justify retaining only the leading term in the expansion of the exponential in (2); in fact, at 200 eV the expansion parameter 2n in Eqs. (2) and (3) equals $\frac{1}{2}$. In other words, at 200 eV the energy still is too low to be confident of the argument--via expansion of $e^{i\chi}$ in (2)--which seemingly reduces the formula (1) to the FBA scattering amplitude. Still, 2n is not large compared to unity at 200 eV; moreover, it is curious that the Glauber and FBA should be so divergent at wide angles in Fig. 10b, in view of the fact that for elastic scattering the 200 eV Glauber and FBA predictions are indistinguishable[4] for angles exceeding 30^{o}. We stress that even without normalization to the same value at $\theta = 21^{o}$, the FBA and Glauber integrated cross sections from Fig. 10b

will be practically equal, as we already know from Figs. 2 and 4 at 200 eV. In other words, the angles where the FBA and Glauber curves of Fig. 10b diverge widely unquestionably are quite inconsequential for purposes of computing the 200 eV total cross section for excitation to the H n = 2 levels, as can be directly verified from Fig. 10b (and its extrapolation to $\theta = 0^{o}$).

For the purposes of the next subsection, it is desirable to assure ourselves that the divergence at large scattering angles between the FBA and Glauber angular distributions of Fig. 10 is consistent with Fig. 8. At E_i = 200 eV, or 100 eV, the FBA and Glauber $|\bar{F}|^2$ shown in Fig. 8 lie close to each other only for $q^2 < \sim 3$; at larger q^2 the FBA $|F|^2$ becomes very small compared to the Glauber. Now at 200 eV, $q^2(\theta)$--which increases monotonically with θ at fixed E_i--equals 3 at about $\theta = 25^{o}$. Thus the angular range for which the FBA and the Glauber predict very nearly the same 1s - 2s differential cross sections at 200 eV is largely off scale in Fig. 10b. At 100 eV, $q^2(\theta) = 3$ at about $\theta = 40^{o}$, so that curves 2 and 3 in Fig. 10a do not begin to diverge until θ exceeds 40^{o}. Actually, it is not possible to understand Figs. 10a and 10b solely from the 1s - 2s curves of Fig. 8, because 1s - 2p excitation contributes importantly to Fig. 10. However, the variation with q^2 of the 1s - 2p $d\sigma/d\Omega$ is not qualitatively dissimilar from the corresponding variation of the 1s - 2s $d\sigma/d\Omega$, as Fig. 7 indicates, so that concentrating solely on the behavior of the 1s - 2s curves of Fig. 8 does yield qualitatively correct interpretations of Figs. 10a and 10b.

4.5 Conclusions and Critique

From the results which have been discussed, it is legitimate to conclude that the Glauber theory is a useful fairly accurate means of

predicting total cross sections for excitation of atomic hydrogen by electrons, at energies 30 eV < E_i < 200 eV; in fact, in this energy range, if theories of e - H excitation are judged on any reasonably weighted combination of reliability, ready computability and theoretical soundness, no other theory seems at all competitive with the Glauber. Whether similar conclusions would hold for other atoms and other incident projectiles, e.g., e - He and p - H collisions, is a question well worth investigating. For instance, in many electron atoms, where $F_{fi}(\vec{q})$ from Eq. (1) must be integrated over the coordinates $\vec{r}_1, \vec{r}_2, \ldots$, of all the atomic electrons, it is far from obvious that $F_{fi}(\vec{q})$ can be reduced to a readily computable form without subsidiary error-introducing simplifying mathematical approximations.

The angular distribution results we have quoted certainly justify the conclusion that the potential utility of Glauber theory for predictions of inelastic (as well as elastic) differential cross sections in electron-atom collisions cannot be lightly dismissed. As a matter of fact, judging by Figs. 9 and 10, Glauber predictions of differential cross sections--for e - H excitation in the same energy range 30 eV < E_i < 200 eV--are almost as successful as are the Glauber total cross section predictions. At first sight, this last assertion is rather surprising. In Figs. 9 and 10 the main advantage of the Glauber lies in its ability to predict the observed angular distributions at wide scattering angles, where the B-O and FBA differential cross sections are far too low; at smaller angles--as Figs. 7 - 10 indicate--normalized (not absolute) differential cross sections are fitted no better by the Glauber than by the even more readily computable FBA. However, as explained in section 2, our calculations specifically have assumed that the momentum transfer $\vec{q}$ is perpendicular to K_i, i.e., that $\vec{q}$ in Eqs. (1) or (8) lies in

the x,y plane containing $\vec{b}$ and $\vec{s}$. Whether or not the incident energy is high, $\vec{q}$ cannot be perpendicular to $\vec{K}_i$ at the wide angles where FBA fails in Figs. 9 and 10. In other words, it appears that the Glauber predictions are successful in Figs. 9 and 10 at just those angles where Glauber theory might be expected to break down.

On the other hand, the foregoing objection to Glauber theory is specious. In Glauber theory, the phase distortion of the wave function is approximated via integration along a straight line supposedly representing the undeviated path of the incident electron; this is how one arrives at the formula for χ, Eqs. (2) - (3). For wide angle scattering, as Glauber remarks[1,2], it is a poor approximation to suppose the electron path is always parallel to $\vec{K}_i$. A better approximation, which treats the initial and final directions symmetrically, results from the assumption that the electron's undeviated straight line path effectively is parallel to $\frac{1}{2}(\vec{K}_i + \vec{K}_f)$. But, recalling Eqs. (6)

$$\frac{\vec{q}\cdot(\vec{K}_i+\vec{K}_f)}{|\vec{q}|\,|\vec{K}_i+\vec{K}_f|} = \frac{K_i^2-K_f^2}{q\,|\vec{K}_i+\vec{K}_f|} = \frac{2m(\epsilon_f-\epsilon_i)/\hbar^2}{\left[(k_i^2+k_f^2)^2-4k_i^2k_f^2\cos^2\theta\right]^{1/2}} = \frac{(\epsilon_f-\epsilon_i)}{\left[\frac{1}{2}(\epsilon_f-\epsilon_i)^2+4E_iE_f\sin^2\theta\right]^{1/2}} \tag{34}$$

Thus at large scattering angles (not too near $\theta = 180^\circ$), choosing the z-axis along $\frac{1}{2}(\vec{K}_i + \vec{K}_f)$ automatically implies that $\vec{q}$ very nearly lies in the x,y plane at not too low energies. For example, in 1s - 2p excitation at $E_i = 200$ eV, the right side of (34) = ~ 0.05 for $\theta = 30^\circ$. Moreover, at any given fixed scattering angle it can be seen that $\Sigma|F_{fi}(\vec{q},m_f)|^2$ summed over all final magnetic quantum numbers m_f does not depend on the direction of quantization of the final boundstate wave functions $u_f(m_f)$. Therefore the

Glauber differential and integrated e - H(1s) cross sections we have computed are exactly the same as we would have obtained if, at the very beginning--back in Eq. (1)--we had made the (superior at all not too low energies) supposition that the z-axis lies along $\frac{1}{2}(\vec{K}_i + \vec{K}_f)$.

The preceding paragraph has made it understandable that Glauber theory accurately predicts differential cross sections at wide angles and not too small incident energies. It also is possible to understand the fact--remarked in subsection 4.4--that at wide angles the Glauber and FBA elastic differential cross sections[3,4] approach each other with increasing E_i, whereas the Glauber and FBA inelastic $d\sigma/d\Omega$ apparently are increasingly divergent with increasing E_i. At high energies, large angle elastic scattering of electrons from H(1s) results predominantly from close collisions between the incident electron and the proton; the atomic electron has too small a mass (alternatively, has too spread out a wave function) to give large deflections to the incident electron. Similarly, one expects that wide angle inelastic scattering results from interactions of the incident electron with the proton as well as with the atomic electron. In FBA, however, the inelastic scattering produced by the interaction e^2/r' between the incident electron and the proton vanishes because the initial and final bound state wave functions are orthogonal. Therefore the wide angle inelastic scattering in FBA results only from the relatively ineffective electron-electron interaction, which explains why the FBA angular distributions of Figs. 9 - 10 decrease so much more rapidly with increasing angle than do the corresponding[3,4] FBA elastic $d\sigma/d\Omega$. This artificial and misleading elimination of the e^2/r' interaction does not occur in the Glauber. Consequently, one expects--and finds, as comparison of Figs. 9 - 10 with Fig. 1 of Tai et al.[4] shows--that at any

given energy the Glauber wide angle inelastic and elastic $d\sigma/d\Omega$ decrease at about the same rate with increasing angle; the fact that at a given energy the experimental elastic and inelastic $d\sigma/d\Omega$ resemble each other already has been remarked by Williams[37]. Returning to the expansion of $e^{i\chi}$ in powers of χ, it appears from the previously reported calculations[3,4] and from the foregoing discussion that at $E_i > 200$ eV keeping only the linear term in χ is not too bad for wide angle elastic scattering. But for inelastic scattering at a fixed large angle--where the contribution from the electron-electron interaction decreases so rapidly with increasing E_i--the linear term in χ is not really the leading term in the expansion of $e^{i\chi}$ after removal of the e^2/r' interaction by orthogonality, and the Glauber does not approach the FBA as E_i increases. It is relevant to later discussion to note here that when retention of only the linear term in χ is justified, the formula (1) reduces to FBA for each final magnetic sublevel, whatever the quantization direction of the atomic bound states, and whether or not the assumption $\vec{q}\cdot\vec{K}_i = 0$ is valid.

For the inelastic collisions of interest in this paper, where $K_f < K_i$, the assumption that $\vec{q}$ is very nearly perpendicular to $\vec{K}_i$ fails at small scattering angles as well as at large θ. To make these remarks more specific, write

$$\vec{q} = \vec{q}_{\parallel} + \vec{q}_{\perp}$$

where $\vec{q}_{||}$ lies along $\vec{K}_i$, and $\vec{q}_{\perp}$ is the component of $\vec{q}$ perpendicular to $\vec{K}_i$. In terms of θ

$$q_{\parallel} = K_i - K_f \cos\theta$$

$$q_{\perp} = K_f \sin\theta$$

In elastic scattering, where $K_f = K_i$, it is evident that $q_{\parallel}$ becomes neglibible compared to $q_{\perp}$ as $\theta \to 0$, i.e., in elastic scattering the assumption $\vec{q}\cdot\vec{K}_i = 0$ is increasingly valid as $\theta \to 0$ at fixed E_i. When $K_f < K_i$, however, $q_{\perp}/q_{\parallel} \to 0$ as $\theta \to 0$ at fixed E_i, i.e., the vector $\vec{q}$ now becomes increasingly parallel to $\vec{K}_i$ in this limit. Furthermore, as Eq. (34) shows, at small angles and moderate-to-low energies, failure of the assumption $\vec{q}\cdot\vec{K}_i = 0$ cannot be remedied by using $\frac{1}{2}(\vec{K}_i + \vec{K}_f)$ as the z-direction. One can argue that at large K_i the angular range near $\theta = 0$ where $q_{\parallel} \ll q_{\perp}$ fails is too small to make a consequential contribution to the integrated inelastic cross section. As K_i decreases, however, $q_{\parallel} \ll q_{\perp}$ is invalid in an increasing angular range near $\theta = 0$, and eventually this range becomes large enough to be consequential in the integrated cross section. It is probable that this failure of the fundamental assumption $\vec{q}\cdot\vec{K}_i = 0$ near $\theta = 0$ is associated with the rapid dropoff of the Glauber below the data points in Figs. 3 and 4 as the energy decreases below $\sim$ 30 eV. At such low energies, where the whole idea of approximating the incident electron trajectory by a straight line path breaks down, it is not easy to decide quantitatively what kinds of errors the Glauber approximation is producing; but it does seem that under these circumstances supposing that $\vec{q}$ lies wholly in a single x,y plane perpendicular to the entire incident electron trajectory—whether this plane is supposed $\perp$ to $\vec{K}_i$ or to $\frac{1}{2}(\vec{K}_i + \vec{K}_f)$—makes the integral (1) an underestimate of the true $F_{fi}(\vec{q})$. This assertion

is based on the effect of replacing q by $q_\perp < q$ in the expressions for $|F_{fi}|^2$ we have obtained [e.g., in Eq. (18)]; Fig. 8 shows that this replacement increases $|F_{fi}|^2$ at every angle. Actually, this unjustified simple replacement of q by $q_\perp$ is too crude, and at low energies brings the Glauber predictions well above the experimental data in Figs. 3 and 4. Nevertheless, it now seems reasonable that--even if electron exchange is negligible--one should expect the Glauber formula (1) to yield too small inelastic cross sections at those low energies for which the assumptions $\vec{q}\cdot\vec{K}_i = 0$ and $\vec{q}\cdot\frac{1}{2}(\vec{K}_f + \vec{K}_i) = 0$ both fail in a non-negligible range of angles near $\theta = 0$. By way of numerical illustration, we note that for 1s - 2p excitation at $E_i = 30$ eV, the right side of (34) is about 0.4 at 30°.

It has been pointed out in section 3.3 that $F_{fi}(\vec{q})$ is identically zero for excitation to the 2p m = 0 level. One easily verifies that this result implies the polarization fraction P [Eq. (33)] of the Lyman α radiation following 1s - 2p excitation should equal - 1 at all incident electron energies. This result must be wrong, and indeed is quite at odds with the observations of Ott et al.[33], who find $P(E_i)$ decreases monotonically from about + 0.2 to - 0.1 in the energy range 20 eV < E_i < 700 eV. Moreover, these observations[33] of $P(E_i)$ are fairly well fitted by FBA calculations in this same energy range. Because the FBA predictions have not taken into account fine structure and hyperfine effect complications (which cannot be ignored[39]), and because the observations include the effects of cascading, it is possible that the agreement between the FBA and measured $P(E_i)$ really is not as good as it seems. Nevertheless, it is obvious that the Glauber fails badly for the purpose of predicting $P(E_i)$. Since the Glauber has otherwise been so successful, some comments concerning this failure to predict $P(E_i)$ certainly are in order.

Actually the reasons Glauber predicts $P(E_i)$ so poorly at energies as high as 700 eV are not wholly transparent to us, but it is clear that use of $\vec{K}_i$ as the z-axis in our calculations [in Eq. (22), specifically] is the source of the difficulty. As we have explained, for any given fixed $\vec{q}$ our results for $\Sigma|F_{fi}(\vec{q},m_f)|^2$ summed over all m_f should be valid at not too low energies, independent of the axis of quantization of the final bound state wave functions. This invariance does not hold for any given individual $|F_{fi}(\vec{q},m_f)|^2$, however. At not too low energies, therefore, it is possible that the ratio of the individual Glauber partial cross sections $\sigma_{2p,1s}(m_f)$ for excitation to 2p $m_f = 0, \pm 1$ quantized along $\vec{K}_i$ can be quite wrong, even though the sum of these partial cross sections is reasonably accurate at any given θ.

At very high energies, however, where the contribution to the total excitation cross section comes almost entirely from forward scattering, so that there is essentially no distinction between quantizing along $\vec{K}_i$ and quantizing along $\frac{1}{2}(\vec{K}_i + \vec{K}_f)$, the Glauber prediction of $P = -1$ should be correct (always neglecting fine structure, hyperfine structure and cascading). In this limit, moreover, the Glauber and FBA predictions of P should coincide. This ultimate coincidence is implied by the claim, in subsection 3.3, that FBA formulas[13] and numerical calculations[14] indicate the probability of 1s - 2p $m = 0$ excitation at high energies is negligible compared to the probability of 1s - 2p $m = \pm 1$ excitation, with the atomic wave functions quantized along $\vec{K}_i$.

We also can give an independent demonstration of the equivalence of the FBA and Glauber predictions of $P(E_i)$ in the limit $E_i \to \infty$, as follows. In FBA, quantizing along $\vec{q}$, only the 2p $m = 0$ level can be excited. When

this state makes a radiative transition to the 1s state, the angular distribution $Q(\vec{\nu})$ of the emitted radiation is proportional[40] to $\sin^2\psi$, where ψ is the angle between $\vec{q}$ and $\vec{\nu}$, the direction of the outgoing radiation. So

$$Q(\vec{\nu}) \sim 1 - \cos^2\psi = 1 - [\cos^2\theta_q \cos^2\theta_\nu + \sin^2\theta_q \sin^2\theta_\nu \cos^2(\phi_q - \phi_\nu) + 2\sin\theta_q \sin\theta_\nu \cos\theta_q \cos\theta_\nu \cos(\phi_q - \phi_\nu)] \quad (35)$$

where the angles θ_q, θ_ν, etc., are being specified relative to $\vec{K}_1$ as polar axis. Averaging (35) over the azimuth of $\vec{q}$, for fixed $\vec{\nu}$, we have

$$\langle Q(\vec{\nu})\rangle \sim 1 - \cos^2\theta_q \cos^2\theta_\nu - \tfrac{1}{2}\sin^2\theta_q \sin^2\theta_\nu \quad (36)$$

Now at high energies and small scattering angles, the predominant contribution to the excitation is coming from $\vec{q} \perp \vec{K}_1$, as has been explained. So in this limit (36) reduces to

$$\langle Q(\vec{\nu})\rangle \sim 1 - \tfrac{1}{2}\sin^2\theta_\nu = \tfrac{1}{2}(1 + \cos^2\theta_\nu) \quad (37)$$

which is precisely the angular distribution of the radiation one infers[40] for transitions from 2p m = ± 1 to 1s, with no original occupation of the state 2p m = 0. Because it is known[21,33] that the angular distribution $Q(\vec{\nu})$ is uniquely related to the polarization fraction P, we now can conclude that for radiation following 1s - 2p excitation the FBA and Glauber P both eq 1 - 1 in the high energy limit.

Acknowledgements

We are indebted to Dr. A. Temkin and the NASA Goddard Space Flight Center for their cooperation in the performance of the numerical computations. We also wish to thank Dr. V. B. Sheorey for numerous instructive conversations.

References

1. R. J. Glauber, in "Lectures in Theoretical Physics", edited by W. E. Brittin, et al. (Interscience Publishers, Inc., New York, 1959), Vol. I, p. 315.

2. See, e.g., C. Wilkin, in "Summer Institute in Nuclear and Particle Physics" (W. A. Benjamin Inc., New York, 1968).

3. V. Franco, Phys. Rev. Letters 20, 709 (1968), who also gives a selection of references to previous non-atomic applications of Glauber theory and discusses the energy regime in which the Glauber approximation is expected to be most useful.

4. H. Tai, P. J. Teubner, and R. H. Bassel, Phys. Rev. Letters 22, 1415 (1969), and 23, 453 (E) (1969).

5. G. Moliere, Z. Naturforsch, 2a, 133 (1947); Fernbach, Serber, and Taylor, Phys. Rev. 75, 1352 (1949).

6. R. Akerib and S. Borowitz, Phys. Rev. 122, 1177 (1961). See also N. F. Mott and H. S. W. Massey, "The Theory of Atomic Collisions" (Oxford, 1965), pp. 334-338.

7. L. Vainshtein, L. Presnyakov, and I. Sobelman, Soviet Physics, JETP 18, 1383 (1964). See also L. Presnyakov, [redacted] Soviet Physics, JETP 20, 760 (1965); D. Crothers and R. McCarroll, Proc. Phys. Soc. (London) 86, 753 (1965); L. Presnyakov, I. Sobelman, and L. Vainshtein, Proc. Phys. Soc. (London) 89, 511 (1966); K. Omidvar, Phys. Rev. Letters 18, 153 (1967); D. Crothers, Proc. Phys. Soc. (London) 91, 855 (1967).

8. M. Abramowitz and I. A. Stegun, "Handbook of Mathematical Functions", (National Bureau of Standards, 1964), p. 376.

9. G. N. Watson, "A Treatise on the Theory of Bessel Functions", (Cambridge, 1966), p. 410.

10. Reference 8, p. 559.

11. I. S. Gradshteyn and I. M. Ryzhik, "Table of Integrals Series and Products", (Academic Press, New York, 1965), p. 384, formula 3.664 - 1.

12. Reference 8, p. 562, formula 15.4.10.

13. T. Y. Wu and T. Ohmura, "Quantum Theory of Scattering", (Prentice Hall, Englewood Cliffs, New Jersey, 1962), p. 194.

14. K. L. Bell, Proc. Phys. Soc. (London) 86, 246 (1965); K. L. Bell and B. L. Moiseiwitsch, Proc. Roy. Soc. (London), A276, 346 (1963).

15. Reference 8, p. 557, formula 15.2.6.

16. L. A. Vainshtein, Opt. Spectry. USSR, 18, 538 (1965).

17. A. R. Holt and B. L. Moiseiwitsch, Proc. Phys. Soc. (London), B1, 36 (1968).

18. L. A. Vainshtein, Opt. Spectry, USSR, 11, 163 (1961).

19. P. G. Burke, H. M. Schey and K. Smith, Phys. Rev. 129, 1258 (1963).

20. V. I. Ochkur, Soviet Physics, JETP, 18, 503 (1964); M. Inokuti, J. Phys. Soc. Japan 22, 971 (1967).

21. W. E. Kauppila, W. R. Ott and W. L. Fite, Phys. Rev., to be published. We are indebted to these authors for furnishing us their data in advance of publication.

22. B. L. Moiseiwitsch and S. J. Smith, Rev. Mod. Phys. 40, 238 (1968), section 2.12.

23. Reference 22, pp. 288-293.

24. D. Hils, H. Kleinpoppen and H. Koschmeider, Proc. Phys. Soc. (London) 89, 35 (1966). For a discussion of this experiment, and suggested explanations of the fact that it yields cross sections which apparently are too low, see references 21 and 23.

25. W. Lichten and S. Schultz, Phys. Rev. 116, 1132 (1959).

26. P. G. Burke, S. Ormonde and W. Whitaker, Proc. Phys. Soc. 92, 319 (1967); A. Joanna Taylor and P. G. Burke, ibid., p. 336; P. G. Burke, A. J. Taylor and S. Ormonde, ibid., p. 345.

27. Reference 22, sections 2.4 - 2.7 and 3.2.

28. E. U. Condon and G. H. Shortley, "The Theory of Atomic Spectra", (Cambridge, 1967), p. 136.

29. D. G. Hummer and M. J. Seaton, Phys. Rev. Letters 6, 471 (1961).

30. R. L. Long, D. M. Cox, and S. J. Smith, J. Res. Natl. Bur. Std. 72A, 521 (1968).

31. W. L. Fite and R. T. Brackmann, Phys. Rev. 112, 1151 (1958).

32. W. L. Fite, R. F. Stebbings and R. T. Brackmann, Phys. Rev. 116, 356 (1959).

33. W. R. Ott, W. E. Kauppila and W. L. Fite, Phys. Rev., to be published.

34. M. Gryzinski, Phys. Rev. 115, 374 (1959); 138, A305 (1965); 138, A322 (1965); 138, A336 (1965).

35. R. C. Stabler, Phys. Rev. 133, A1268 (1964).

36. N. F. Mott and H. S. W. Massey, "The Theory of Atomic Collisions", (Oxford, 1965), p. 481.

37. K. G. Williams in, "Sixth International Conference on the Physics of Electronic and Atomic Collisions, Abstracts of Papers", (MIT Press, Cambridge, 1969), p. 731. We are indebted to Dr. Williams for sending us his detailed data.

38. B. L. Scott, Phys. Rev. 140, A699 (1965).

39. I. C. Percival and M. J. Seaton, Phil. Trans. Roy. Soc. (London), 251A, 113 (1958).

40. Reference 28, p. 99.

Figure Captions

Figure 1. Projection of the collision on the x,y plane. The x,y plane is the plane of the paper; the initial velocity of the incident electron coincides with the direction of positive z, which is into the paper. The vectors $\vec{b}$, $\vec{s}$, $\vec{q}$ lie in the x,y plane, and have azimuth angles ϕ_b, ϕ_s, ϕ_q respectively, measured from positive x, as shown.

Figure 2. The 1s - 2s excitation cross section, in units of πa_o^2, computed via Glauber and various other approximations discussed in the text. Curve 5 is the Burke, Schey and Smith (reference 19) 1s - 2s - 2p close coupling calculation, including exchange; curve 6 is the Holt and Moiseiwitsch (reference 17) estimate, using closure, of the second Born approximation; curve 7 is the distorted wave approximation.

Figure 3. Comparison of theoretical and experimental effective 1s - 2s excitation cross sections, in units of πa_o^2. Solid circles, the data points of reference 21, normalized to FBA at 200 eV; crosses, the data points of reference 24, normalized to FBA at 500 eV. Solid curve, the Glauber predictions; dashed curve, the first Born approximation. As explained in the text, in order that comparison with the data be meaningful, the theoretical curves must plot $\sigma_{2s,1s} + \gamma \sigma_{3p,1s}$, where γ has been estimated to equal 0.23.

Figure 4. The 1s - 2p excitation cross section, in units of πa_o^2. The triangles are the data points of reference 30. The curves show various theoretical estimates of 1s - 2p excitation, computed via Glauber and various other approximations discussed in the text. The sources for the theoretical curves are as in Fig. 2, e.g., curve 5 is the 1s - 2s - 2p close coupling calculation, including exchange, from reference 19.

Figure 5. Total cross section for excitation to the n = 2 levels of hydrogen, in units of πa_o^2. The triangles are the observations, taken from Figs. 3 and 4 as explained in the text. Solid curve, the Glauber predictions, from Figs. 3 and 4; dashed curve, the first Born approximation, from Figs. 3 and 4; dot-dashed curve, the Gryzinski classical model, as computed in reference 35.

Figure 6. Theoretical 1s - 3s and 1s - 3p cross sections, in units of πa_o^2. Solid curves, the Glauber predictions; short dashed curves, the first Born approximation; long dashed curves, the distorted wave approximation; dotted curve, a 1s - 3p close coupling calculation (reference 19).

Figure 7. Theoretical differential cross sections, in units of πa_o^2, for excitation to 2s, 2p, 3s and 3p, at 100 eV. Solid curves, the Glauber predictions; dashed curves, the first Born approximation.

Figure 8. Scattering amplitude squared, in units of πa_o^2, for 1s - 2s excitation, as a function of q^2 = momentum transfer squared. Solid curves, the Glauber predictions, at energies of 50, 100 and 200 eV; dashed curve, the first Born approximation, which is independent of incident energy.

Figure 9. Differential cross sections for excitation of the n = 2 levels of atomic hydrogen. Curve 1, data points of Williams, reference 37. Curves 2, 3 and 4 are theoretical angular distributions, all normalized to the experimental data points at $\theta = 20^o$. Curve 2, the 1s - 2s - 2p close coupling predictions; curve 3, the Born-Oppenheimer approximation; curve 4, Glauber.

Figure 10. Differential cross sections for excitation of the n = 2 levels of atomic hydrogen (a) at 100 eV; (b) at 200 eV. Curves 1, data points of reference 37. Curves 2 and 3 are theoretical angular distributions, all normalized to the experimental data points at $\theta = 21^{\circ}$. Curve 2 (dashed), the Born-Oppenheimer approximation; curve 3 (solid), Glauber.

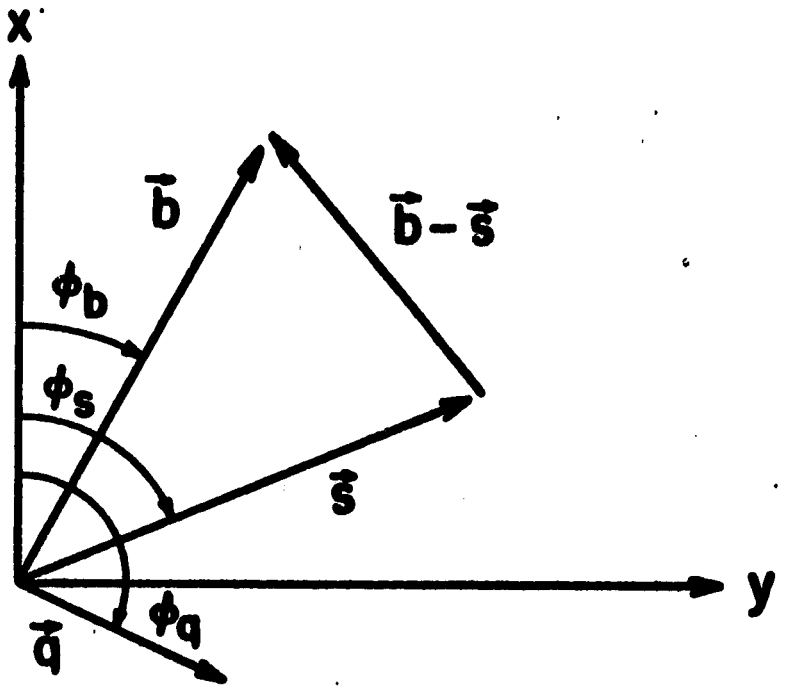

Figure 1

Figure 2

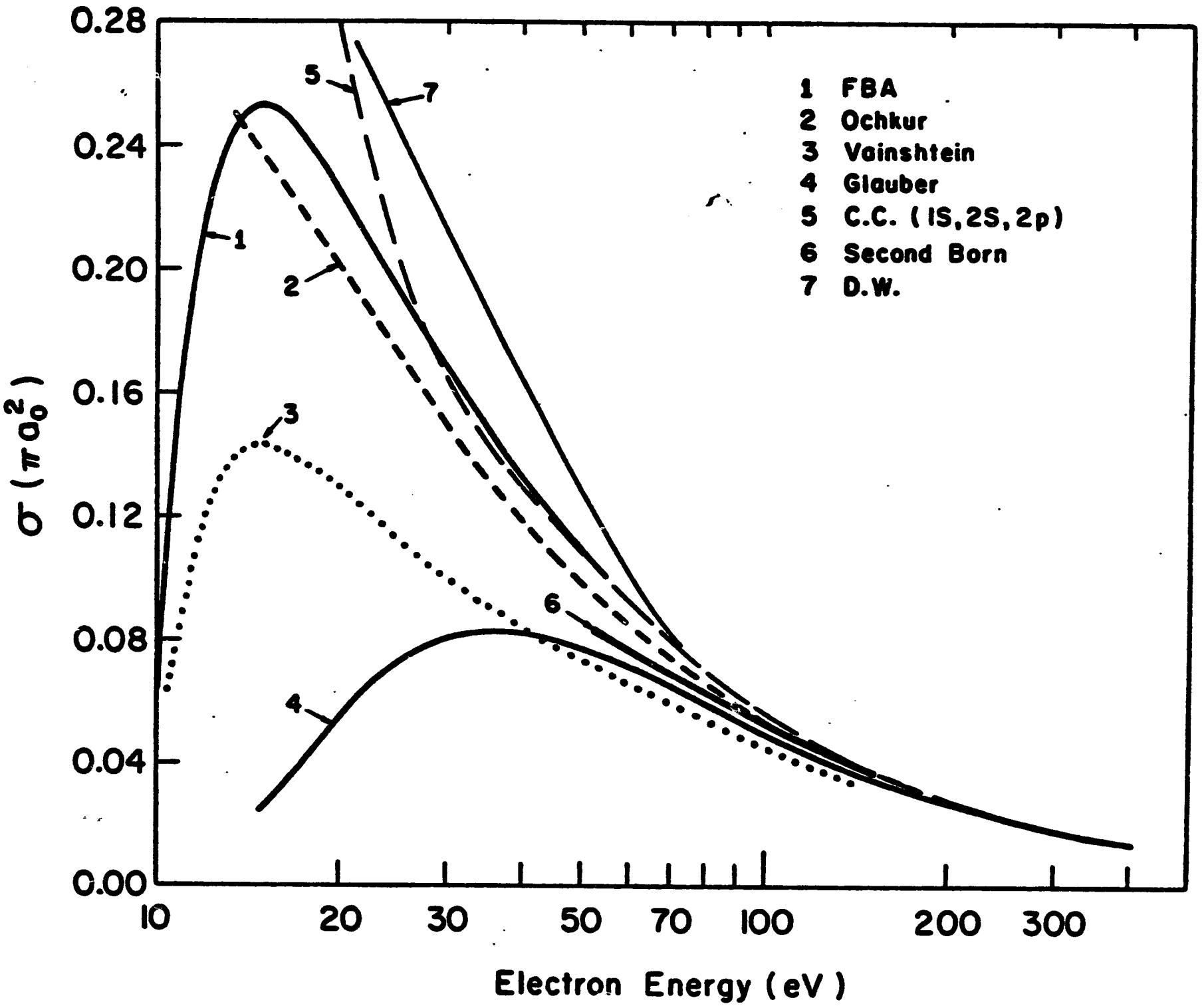
0.28
0.24
0.20
0.16
0.12
0.08
0.04
0.00
σ (πa₀²)
10
20
30
50
70
100
200
300
Electron Energy (eV)
1 FBA
2 Ochkur
3 Vainshtein
4 Glauber
5 C.C. (1S, 2S, 2p)
6 Second Born
7 D.W.

Figure 5

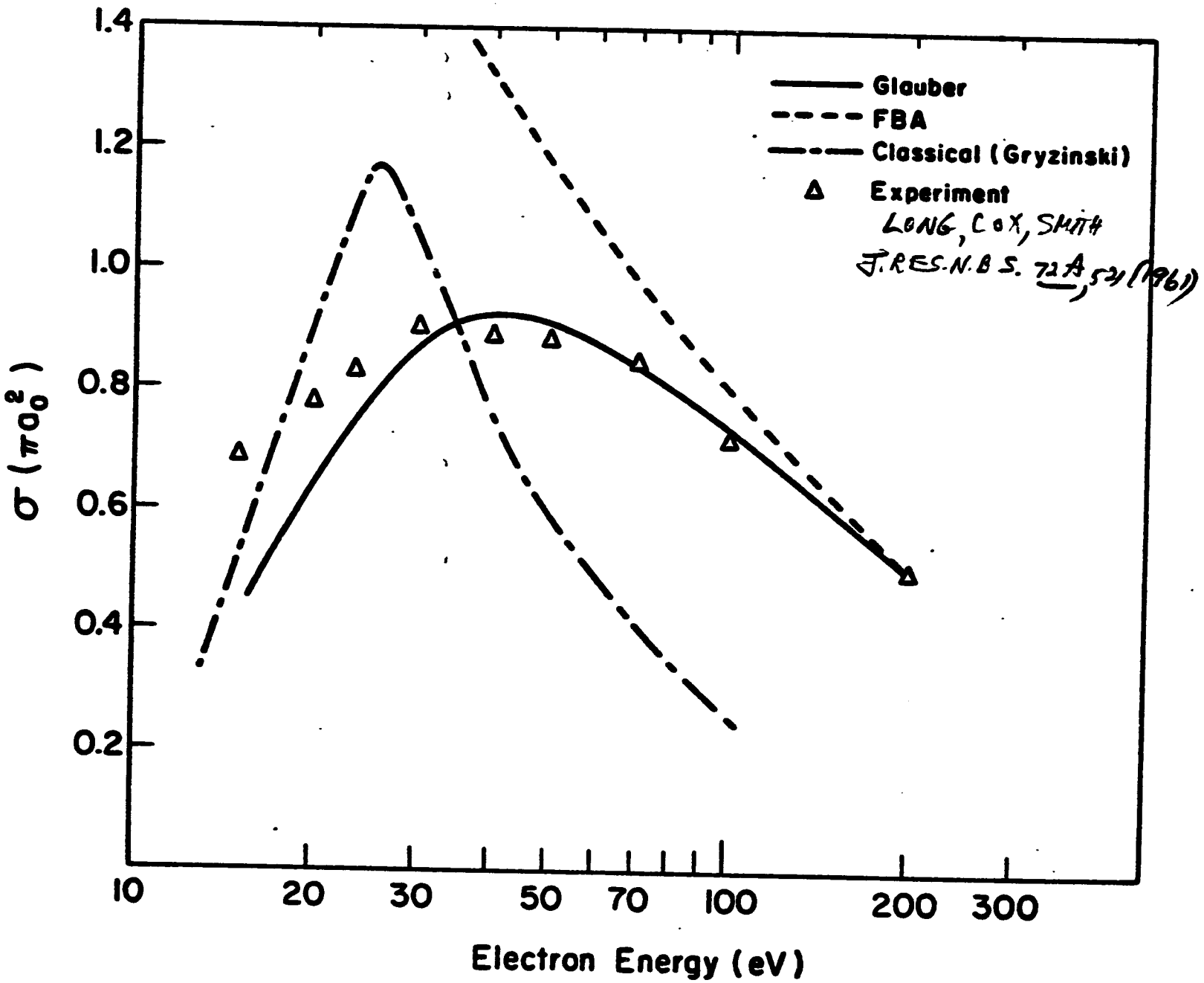

Figures 3, 4 missing
PRECEDING [redacted] NOT FILMED

Figure 6

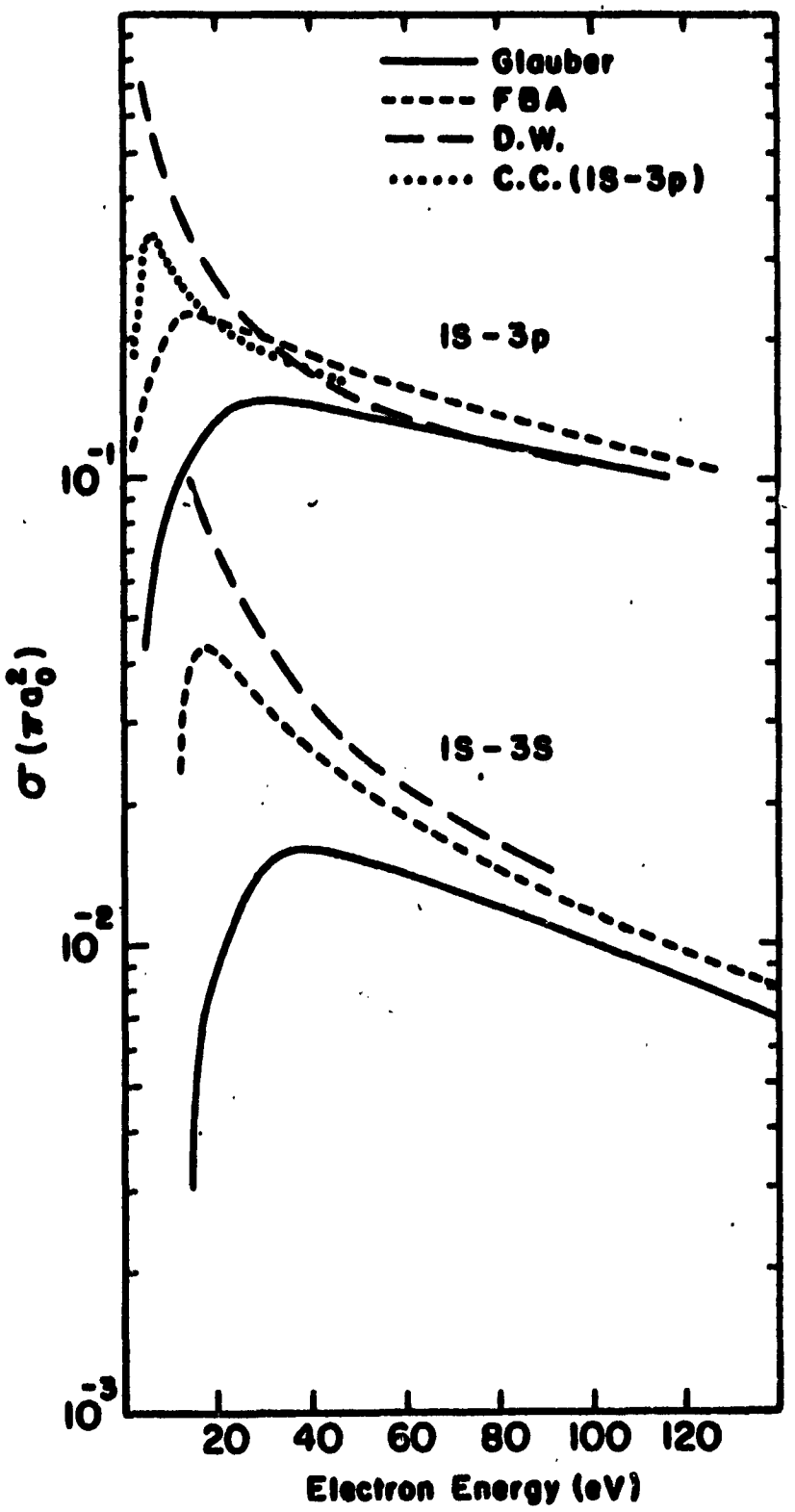
Glauber
FBA
D.W.
C.C.(1S-3p)
1S-3p
1S-3S
10^{-1}
10^{-2}
10^{-3}
$\sigma(\pi a_0^2)$
20
40
60
80
100
120
Electron Energy (eV)

Figure 7

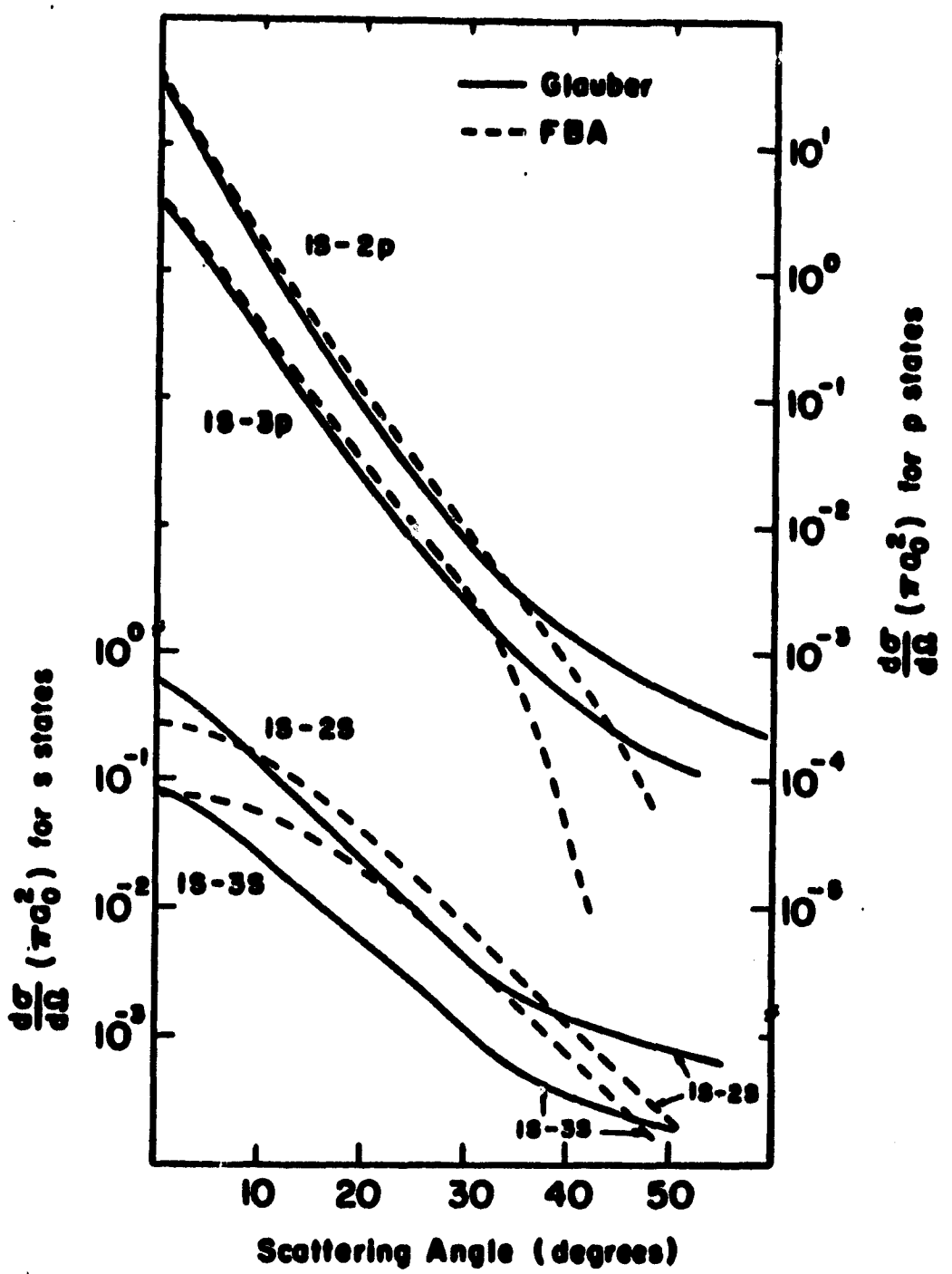
Glauber
FBA
1S-2p
1S-3p
1S-2S
1S-3S
1S-2S
1S-3S
10
20
30
40
50
Scattering Angle (degrees)
$\frac{d\sigma}{d\Omega}$ (πa_0^2) for s states
$\frac{d\sigma}{d\Omega}$ (πa_0^2) for p states

Figure 8

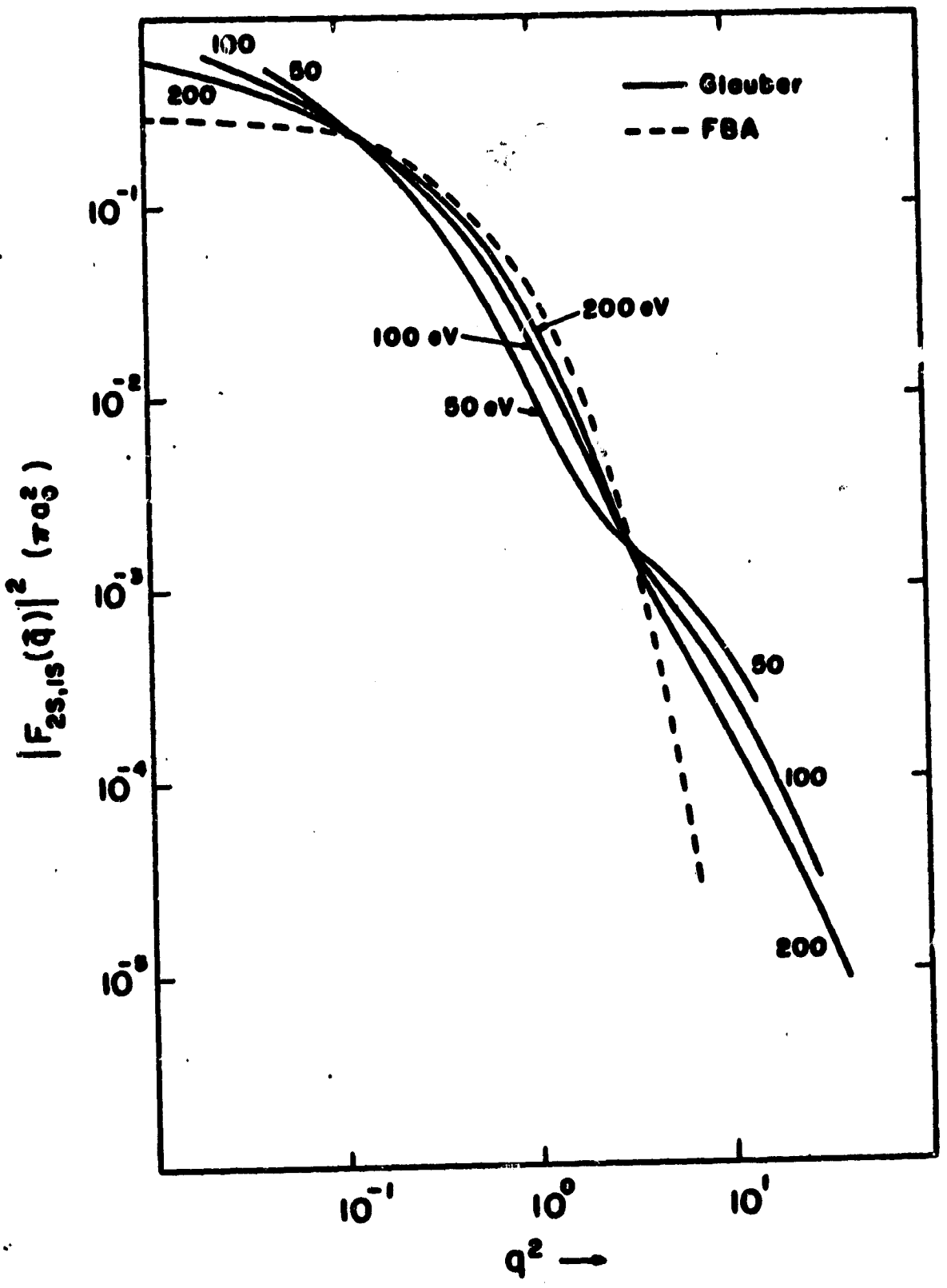
100
50
200
Gleuter
FBA
10^{-1}
10^{-2}
10^{-3}
10^{-4}
10^{-5}
200 eV
100 eV
50 eV
50
100
200
10^{-1}
10^{0}
10^{1}
q^2 ⟶
$|F_{2s,1s}(q)|^2$ (πa_0^2)

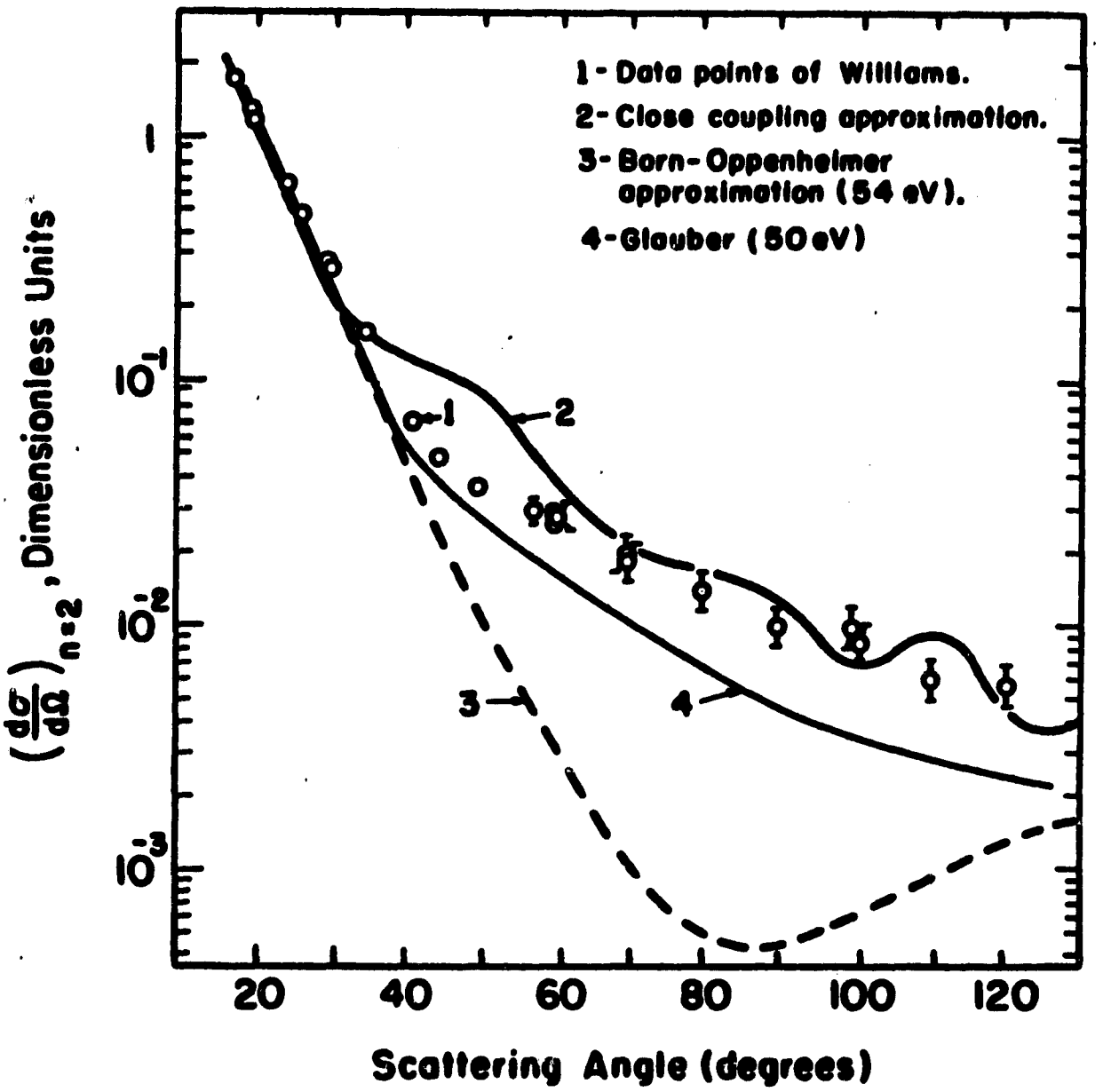
1 - Data points of Williams.
2 - Close coupling approximation.
3 - Born - Oppenheimer approximation (54 eV).
4 - Glauber (50 eV)
1
10^{-1}
10^{-2}
10^{-3}
$\left(\frac{d\sigma}{d\Omega}\right)_{n=2}$, Dimensionless Units
20
40
60
80
100
120
Scattering Angle (degrees)

Figure 9

Figure 10

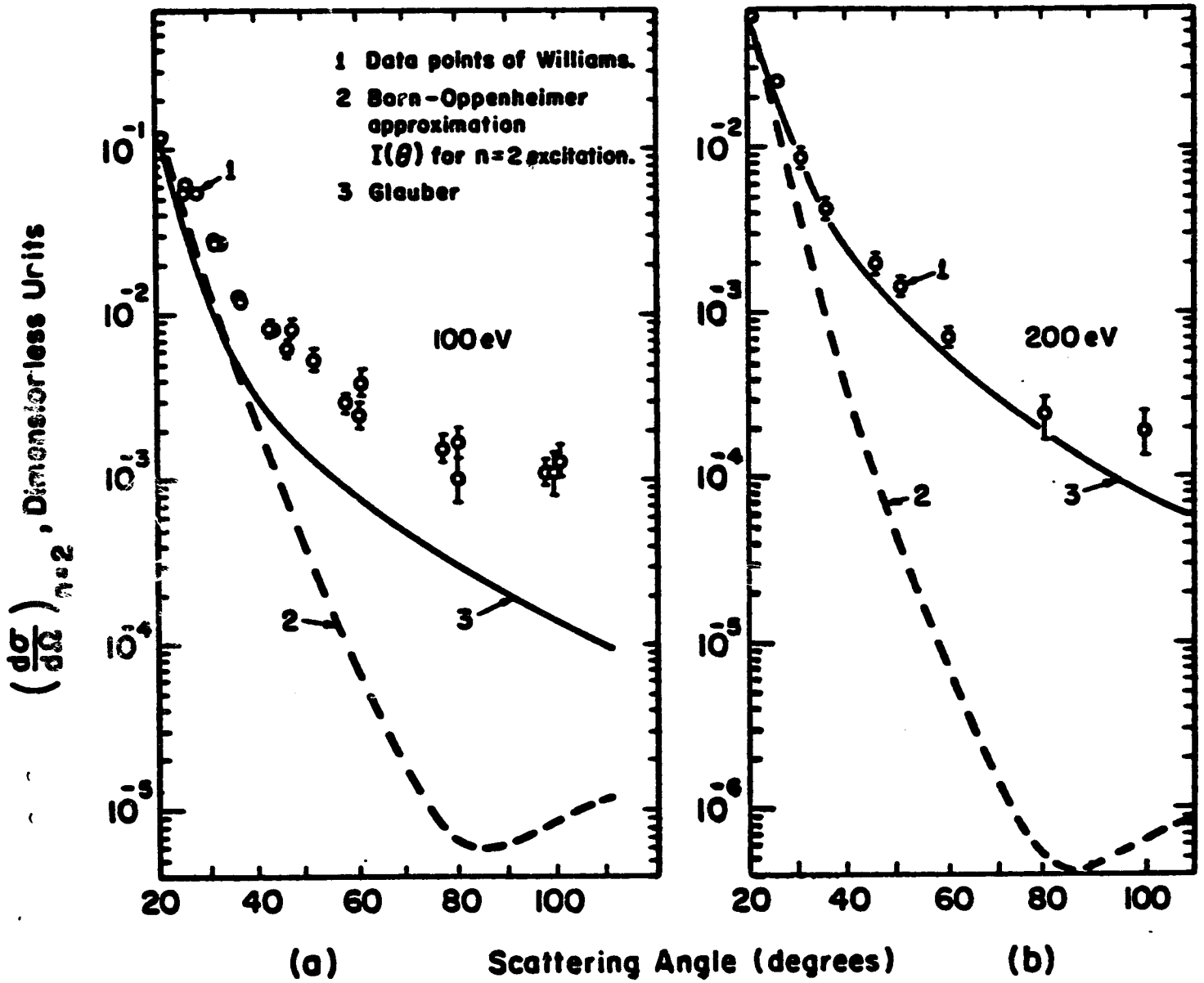
1 Data points of Williams.
2 Born-Oppenheimer approximation I(θ) for n=2 excitation.
3 Glauber
100 eV
200 eV
$\left(\frac{d\sigma}{d\Omega}\right)_{n=2}$, Dimensionless Units
10^{-1}
10^{-2}
10^{-3}
10^{-4}
10^{-5}
10^{-6}
20
40
60
80
100
(a)
Scattering Angle (degrees)
(b)